BURNING RATE CHARACTERIZATION OF AMMONIUM PERCHLORATE PELLETS CONTAINING MICRO- AND NANO-CATALYTIC ADDITIVES

A Thesis

by

FELIX ALEJANDRO RODRIGUEZ

Submitted to the Office of Graduate and Professional Studies of
Texas A&M University
in partial fulfillment of the requirements for the degree of

MASTER OF SCIENCE

Chair of Committee,	Eric L. Petersen
Committee Members,	Dorrin Jarrahbashi
	Adonios Karpetis
Head of Department,	Andreas A. Polycarpou

May 2020

Major Subject: Mechanical Engineering

ABSTRACT

Ammonium perchlorate (AP) is an extensively used oxidizer in solid composite propellants, and its combustion behavior can be tailored by the presence of catalytic additives such as metal oxides. Nano-sized metal oxide catalysts have been utilized in place of their micro-sized counterparts to tailor burning rates of composite Ammonium Perchlorate (AP)/Hydroxyl-terminate Polybutadiene (HTPB) propellants. The effects of micro- and nano-sized metal oxide catalysts on the combustion of AP were investigated and thoroughly characterized herein.

AP pellets were manufactured with micro- and nano-iron oxide (Fe_2O_3) and micro- and nano-titanium oxide (TiO_2) at several mass loadings (0-3% by mass) and were burned from 3.45-34.5 MPa (500-5,000 psi) in a constant-volume strand bomb. Intimate contact between the AP and micro- or nano-catalysts was ensured using a Resonant Acoustic Mixer (RAM). The homogenous mixture of AP and catalyst was pressed into pellets using a Carver hydraulic press. The sides of the pellets were inhibited prior to burning to discourage side-wall burning.

The incorporation of 1% μFe_2O_3 yielded the highest burning rate among all formulations herein within the investigated pressure range. The incorporation of $nTiO_2$ and nFe_2O_3 yielded burning rates which were independent of mass loading within the range of evaluated conditions (0.25-1%). All micro-formulations investigated increase the burning rate at pressures ranging from roughly 13.45- 17.24 MPa (1,950-2,500 psi) and 4.50-8.60 MPa (650-1,250 psi) and for μTiO_2 and μFe_2O_3, respectively; and these

effects were dependent on the catalyst mass loading. The nano-formulations increased the burning rate at pressures greater than 11.27 (1,620 psi) and 8.27 MPa (1,200 psi) for $nTiO_2$ and nFe_2O_3, respectively. The low-pressure deflagration limit (LPDL) is observed at higher pressures for samples containing the nano-additives in comparison to samples containing micro-additives. The occurrence of a LPDL was attributed to radiative heat transfer losses. Future testing efforts will be geared towards the characterization of AP pellets with energetic additives such as aluminum, boron, and zirconium.

ACKNOWLEDGMENTS

I would like to acknowledge and thank Dr. Eric Petersen for the opportunity to continue my education as a member of his research group. Through his guidance as an advisor and professor, he has helped me increase my knowledge and research experience exponentially in the past two years. I would also like to acknowledge my fellow researchers and friends: James Thomas, Thomas Sammet, Catherine Dillier, David Teitge, and Erica Petersen, each person listed has contributed to this research in some way. In particular, James Thomas was instrumental in all ballistic testing and material characterization, while Thomas Sammet was instrumental in sample formulation and ballistic testing as well. Additionally, I would like to thank Dr. Dorrin Jarahhbashi and Dr. Adonios Karpetis for acting as members on my committee.

Lastly, I would like to thank my family, Felix I. Rodriguez, Silka E. Rodriguez and Diana Rodriguez for supporting me in all endeavors. I love you and appreciate everything you have done and continue to do for me.

CONTRIBUTORS AND FUNDING SOURCES

This work was supported by a thesis committee consisting of Professors Eric Petersen and Dorrin Jarahhbashi of the Department of Mechanical Engineering and Professor Adonios Karpetis of the Department of Aerospace Engineering. I would like to thank American Pacific (AMPAC) for donating the plain Ammonium Perchlorate (AP) used in all formulations herein.

I would also like to acknowledge Dr. Eric Petersen and the Turbomachinery lab for funding this research.

NOMENCLATURE

μAl	Micro-Aluminum
μFe_2O_3	Micro-Iron Oxide
μTiO_2	Micro-Titanium Oxide
AMPAC	American Pacific
AP	Ammonium perchlorate
BSE	Back-Scatter SEM
$BKNO_3$	Boron Potassium Nitrate
CuO	Copper Oxide
DAQ	Data acquisition
EDS	Energy Dispersive Spectroscopy
Fe_2O_3	Iron Oxide
HTPB	Hydroxyl-terminate Polybutadiene
HRC	Rockwell hardness C
IPDI	Isophorone Diisocynate
l	Length
LPDL	Low-Pressure Deflagration Limit
nAl	Nano-Aluminum
nFe_2O_3	Nano-Iron Oxide
$nTiO_2$	Nano-Titanium Oxide
PTFE	Polytetrafluoroethylene
PDL	Pressure deflagration limit

r	Burning rate
RAM	Resonant acoustic mixing
RSS	Root-Sum-Squares
SEM	Scanning electron microscope
t	Time
TEM	Transmission Electron Microscopy
TiO_2	Titanium Oxide
TMD	Theoretical Max Density
UPDL	Upper Pressure Deflagration Limits

TABLE OF CONTENTS

Page

LIST OF FIGURES

Page

LIST OF TABLES

Page

1. INTRODUCTION*

Solid propellants have a wide range of applications in industries ranging from missile propulsion to space exploration [1]. A solid propellant can be optimized for a specific application through the addition of various additives. Catalytic and energetic additives can be used to enhance burning rates, while bonding agents and plasticizers can be used to tailor mechanical properties. A fuel and oxidizer are the main components of a solid propellant. In the propulsion community, one of the most commonly used fuel and oxidizer pairs is hydroxyl-terminated polybutadiene (HTPB) and ammonium perchlorate (AP). These materials are heterogeneously mixed together and a curative, isophorone diisocynate (IPDI), is added to cause the HTPB to have a rubber consistency. The fuel and oxidizer will remain unreacted in this state and remain as such until an ignition source is applied. Upon ignition, the fuel and oxidizer will continue to react until all the material has been consumed by the combustion process. The elevated pressure and temperature byproduct gases can then be used for propulsive purposes.

There are two classifications for solid propellants: double base and composite propellants. A typical double base propellant consists of liquid nitroglycerine and nitrocellulose. A small percentage of additives can be absorbed into nitrocellulose

* Parts of this section is reprinted from "Burning Rate Characterization of Ammonium Perchlorate Pellets Containing Catalytic Additives" with permission from Rodriguez, F. A., AIAA 2019-4440, 2019 AIAA Joint Propulsion Conference, Indianapolis, IN, 2019, and from "Burning Rate Characterization of Ammonium Perchlorate Pellets Containing Nano-Catalytic Additives" with permission from Rodriguez, F. A., AIAA 2020-1425, 2020 AIAA Science and Technology Conference, Orlando, FL, 2020.

creating a homogenous propellant grain. Nitrocellulose and liquid nitroglycerine are both highly energetic and contain fuel and oxidizer components [1]. A composite propellant is typically a heterogeneous mixture of fuel and oxidizer that is held together by a curing agent, oven-cured binder, or pressed into a pellet. The burning rates of these composite propellants can be tailored through the addition of metals and metal oxides.

AP is used extensively as the oxidizer component of composite propellants and plays a significant role in the overall performance. Gaining a deeper understanding of the effects a metal oxide catalyst has on the burning rate of AP alone can allow for better control over composite propellants. The purpose of this thesis was to characterize the burning rates of AP pellets with nano- and micron-sized metal oxide catalytic additives. This characterization was done by performing ballistic testing and microscopy on AP pellets with iron oxide (Fe_2O_3) and titanium oxide (TiO_2) in both micro- and nano-sized forms.

The following sections of this thesis provide a brief literature review of previous AP pellet studies with additives, as well as several sources showing the discrepancy in the literature regarding micro- vs nanoparticles. Following this, the pellet formulation and experimental setup and procedure are detailed. Next, the catalyst and select samples were characterized through SEM, TEM, and EDS analyses. The ballistic experiment results and discussion follow, including pertinent comparisons to previous studies. With all the ballistic testing analysis complete, conclusions and recommendations for future work are detailed.

2. LITERATURE REVIEW*

2.1 Metal Oxides in Solid Propellants

The inclusion of metal oxides, such as iron oxide (Fe_2O_3) and titanium oxide (TiO_2), in composite AP/HTPB propellants has been observed to increase the global burning rates [2-15]. It is well documented in the literature that metal oxides enhance the thermal decomposition of AP [16]. Wang et al. [17] conducted strand burner experiments with nano-sized CuO, Fe_2O_3, and composite CuO/Fe_2O_3 additives incorporated in composite AP/HTPB propellants, with the Fe_2O_3 formulation increasing the burning rate 66% over the baseline. Stephens et al. [13] utilized a Taguchi L8 matrix to compare multiple parameters in solid composite propellants including additive type, concentration, and size. Their study showed the burning rate had high sensitivity to the additive type, and TiO_2 outperformed CeO_2. Krietz et al. [10] included TiO_2 in composite propellants through several different mixing and preparation methods. Subsequent ballistic testing indicated that intimate contact between the catalyst and other propellant components plays an important role in determining the resultant combustion behavior. More explicitly, the incorporation of TiO_2 showed an increase in burning rate over the corresponding baseline only when intimate contact was achieved. These studies

* Parts of this section is reprinted from "Burning Rate Characterization of Ammonium Perchlorate Pellets Containing Catalytic Additives" with permission from Rodriguez, F. A., AIAA 2019-4440, 2019 AIAA Joint Propulsion Conference, Indianapolis, IN, 2019, and from "Burning Rate Characterization of Ammonium Perchlorate Pellets Containing Nano-Catalytic Additives" with permission from Rodriguez, F. A., AIAA 2020-1425, 2020 AIAA Science and Technology Conference, Orlando, FL, 2020.

verified that the addition of Fe_2O_3 and TiO_2 have positive effects on the AP/HTPB composite propellant system.

2.2 Nano- versus Micro-sized Particles in Solid Propellants

A study reported by Kshirsagar et al. [18] investigated the effects of nano- and micro-manganese dioxide (MnO_2) in composite propellants. Both sizes of the additive increased the burning rates relative to the baseline, but there was only a 2% increase in burning rate from the micron formulation to the nano-formulation. Determining whether or not this increase is significant is subject to the interpretation of the reader. Reid et al. [15] conducted a study incorporating nano-scale TiO_2 into AP/HTPB composite propellants. Several different forms of the catalyst were used (rutile, anatase, and amorphous) with particle sizes ranging from 15 to 200 nm. The maximum increase in burning rate was reported to be 30% relative to the baseline formulation. Marothiya et al. [19] reported a study using AP with nFe_2O_3 embedded on the surface in aluminized composite propellants. The catalyst was incorporated on the micro- and nano-scale and resulted in an increased burning rate of 27.4% and 7.3%, respectively. Stephens et al. [20] investigated the effects of nano-aluminum (nAl) and micron-aluminum (μAl) on AP/HTPB composite propellants and arrived at the conclusion that other factors affect whether nAl causes an increase in burning rate, such as AP concentration and size. It can be extrapolated from the literature that the positive effects of nano-scale particles over their micro-scale counterparts are situationally dependent.

2.3 AP Pellet with Additive Studies

Additional investigations of the effect Fe_2O_3 has on reagent and plain AP alone have been conducted previously. Friedman et al. [21] investigated the deflagration rate of AP pellets pressed from reagent-grade AP of varying particle sizes and preparation methods. The particle sizes utilized therein ranged from a few microns to a few hundred microns, and AP was utilized in the 'as-received' condition and after being sieved to specific size ranges. Rectangular pellets (4 × 4 × 38 mm) were manufactured using a hydraulic press (100 ksi) and pellet punch system. The densities of the pellets were seen to deviate from the single-crystal value as the particle size was decreased. The highest density achieved in this study was 1.908 g/cc, which is approximately 97.8% of the single-crystal density. Burning rate data were gathered using a nitrogen-pressurized strand burner coupled with a hot-wire ignition system. Several timing fuse wires and motion-picture photography were used to track the flame propagation through the pellets. Testing of the "as received" AP resulted in upper and lower deflagration limits of 45 atm (660 psi) and 300 atm (4,400 psi), respectively. Testing completed with the sieved AP resulted in a decreased region of burning rate data, the lower deflagration limit moved to a higher pressure and the upper deflagration limit moved to a lower pressure. The disagreement associated with the sieved and 'as-received' samples was attributed to the lower densities in the sieved AP. Accordingly, the 'as-received' samples were chosen for further testing. Several catalysts were incorporated into the AP pellets at a mass loading of 3%. μFe_2O_3 was found to decrease burning rates at lower pressures and increase burning rates at higher pressures. The crossover point where μFe_2O_3 began

to have a positive catalytic effect was approximately 116 atm (1,700 psi). The concentration of μFe_2O_3 was not investigated further due to copper chromite formulations yielding the highest burning rate.

Boggs et al. [22] studied the combustion of single-crystal AP and pellets pressed from 99.9% pure AP with particle sizes ranging from 44 to 77 μm. Pellets (2 × 6 × 10 mm) were manufactured using a hydraulic press which applied a force of 48,600 psi for 30 minutes. Experiments were conducted in a stainless-steel window bomb with pressurization capabilities up to 2,000 psi. A braided nichrome wire was used to achieve sample ignition. Burning rate data were extrapolated using a high-speed camera. This testing methodology was implemented with single-crystal AP samples and resulted in a low degree of scatter. The same low degree of scatter did not translate to the AP with additive-pressed pellet experiments due to nonuniform burning of the additive pellets and not the measurement precision. Additive formulations were manufactured with μFe_2O_3 at 2% and 8% concentration by mass, and the 2% μFe_2O_3 pellets yielded an increase in the deflagration rate and temperature sensitivity of pure AP. The 8% concentration decreased the burning rate and altered the low-pressure deflagration limit to a higher pressure than plain AP. Further experimentation into the optimal percentage of μFe_2O_3 was not conducted.

Marothiya et al. [23] conducted strand burner experiments with AP pellets comparing the effects of mechanically mixed and embedded catalysts. The embedding process consisted of dissolving the AP in water, filtering out any impurities, mixing in the appropriate amount of catalyst, and evaporating the water out slowly, which resulted

in catalyst-embedded AP. The process of embedding the AP with catalyst was completed with μFe_2O_3 from several different suppliers. Pellets were shaped into rectangles using a surgical knife, and five of the six faces were inhibited with silica grease. The samples were then burned at 70 bar (~1,000 psi) in a Crawford bomb. μFe_2O_3 loading percentages were varied from 0.75-5%. The burning rate of the 1% catalyst loading was the highest, which was reported to agree with the literature. The catalytic effect of μFe_2O_3 decreased as the concentration was increased to 5%. An optimal concentration was thought to reside between 0.75 and 1% μFe_2O_3. Multiple suppliers were used for the embedded catalyst samples, and even at the same concentrations different burning rates were observed. This observation alludes to the importance of additive characterization.

In summary, metal oxides have been well established as burning rate modifiers for solid propellants, but the parameters that control these mechanisms have not been adequately characterized in the literature. In the current study, Fe_2O_3 and TiO_2 were implemented at various particle sizes and loadings in AP pellets to investigate their potential catalytic effects on pure AP, thereby removing any complications that may arise when considered a more-complex composite propellant formulation containing HTPB and other additives in addition to the metal oxides.

3. EXPERIMENTAL METHODOLOGY*

3.1 Propellant Formulations

The AP utilized herein was high-purity (> 99.9%) and donated by American Pacific (AMPAC) with an average particle size of approximately 250 μm. Previous studies completed by Seetharamacharyulu et al. [24] concluded that the burning rate of AP pellets is independent of the particle size of the AP particles used once the TMD of the AP pellets exceeds 98%. The threshold of 98% TMD can be reached by varying the pressing parameters, such as compaction force and dwell time. The average density for each formulation evaluated herein is given in Table 1. The average %TMD for all pellets investigated was above about 98%, and this exceeds the threshold previously mentioned.

* Parts of this section is reprinted from "Burning Rate Characterization of Ammonium Perchlorate Pellets Containing Catalytic Additives" with permission from Rodriguez, F. A., AIAA 2019-4440, 2019 AIAA Joint Propulsion Conference, Indianapolis, IN, 2019, and from "Burning Rate Characterization of Ammonium Perchlorate Pellets Containing Nano-Catalytic Additives" with permission from Rodriguez, F. A., AIAA 2020-1425, 2020 AIAA Science and Technology Conference, Orlando, FL, 2020.

Table 1 Formulation details and average measured densities for all samples evaluated herein.

Formulation	Additive	Additive (wt %)	Density (g/cm^3)		
			Theoretical	Actual	%
1	None	-	1.95	1.92	98.5
2	μTiO_2	1	1.96	1.92	98.0
3	μTiO_2	2	1.97	1.93	98.2
4	μTiO_2	3	1.98	1.94	98.0
5	μFe_2O_2	0.5	1.96	1.91	97.7
6	μFe_2O_2	1	1.96	1.92	97.9
7	μFe_2O_2	2	1.97	1.93	98.1
8	μFe_2O_2	3	1.99	1.95	98.1
9	$nTiO_2$	0.25	1.95	1.92	98.4
10	$nTiO_2$	0.5	1.96	1.92	97.7
11	$nTiO_2$	1	1.96	1.92	97.9
12	nFe_2O_2	0.25	1.95	1.91	98.1
13	nFe_2O_2	0.5	1.96	1.92	97.9
14	nFe_2O_2	1	1.96	1.92	98.5

The loading percentage of the micro-catalysts were initially varied from 1-3%. An additional 0.5% μFe_2O_3 formulation was tested to investigate the potential existence of a catalytic loading and performance threshold. The micro-catalyst experiments yielded the trend that as the loading percentage was decreased, the burning rate would increase. Due to this trend, the loading percentage of the nano-catalysts was varied from 0.25 to 1%.

The amount of homogeneous material needed to make a 0.5″ × 0.5″ pellet varies due to the variety of loading percentages and materials being used. The required masses for each formulation can be seen in Table 2. The densities for the materials used were as follows; 1.95, 5.24, and 4.23 g/cm^3 for the plain AP, Fe_2O_3, and TiO_2 additives, respectively.

Table 2 Theoretical densities and required mass per pellet for each formulation.

Formulation	Mass Loading (%)	Theoretical Density (g/cm^3)	Required Mass per Pellet (g)
Baseline	0	1.95	3.21
μ-TiO_2	1	1.96	3.22
	2	1.97	3.24
	3	1.98	3.26
n-TiO_2	0.25	1.95	3.21
	0.5	1.96	3.22
	1	1.96	3.22
μ-Fe_2O_3	0.5	1.96	3.22
	1	1.96	3.23
	2	1.97	3.25
	3	1.99	3.27
n-Fe_2O_3	0.25	1.95	3.21
	0.5	1.96	3.22
	1	1.96	3.23

3.2 Mixing Method

One piece of equipment that the Petersen Research Group has in their facility at the Turbomachinery Laboratory is a Resodyn Resonant Acoustic Mixer (RAM). The RAM utilizes mechanical resonance to transfer large amounts of energy to a heterogenous mixture of powders causing them to violently mix until a homogenous mixture is achieved. The three main mixing parameters that can be altered are: force, mix time, and fill level. The force or mixing intensity can be set to any value between 1 and 100 g's. The mixing time is controlled by a set timer on the device interface that can be set to the desired time. The fill level refers to the amount of material that is put into the vial of choice, a 36-mL plastic vial was used for these formulations. The top and bottom of the vial are used as transducers that promote mixing; if the vial is not filled too

much, the top transducer or vial lid will not play an active role in the mixing process. The use of both top and bottom transducers can be achieved by tailoring the mixing intensity and fill level for a given application. It is worth noting that a glass vial with a slightly larger volume was used to mix a formulation, and there was not a difference in the pellet burning rates. The mixing parameters for the present experiment were as follows: 2-minute mixing time, 70 g's of acceleration, and 75-85% fill [25]. Sufficient material to make 10 pellets was weighed and placed into 36-mL plastic vials for mixing. The RAM mixer can be seen in Fig. 1.

The RAM utilizes resonance frequency and ultrasonic sound waves to bring the system to a constantly monitored and changing resonant condition. Once this condition is achieved, the top and bottom of the vial become transducers which increase collisions among particles along with sidewall and particle-to-particle collisions. A schematic of how the RAM is used to create a homogeneous mixture is shown in Fig. 2.

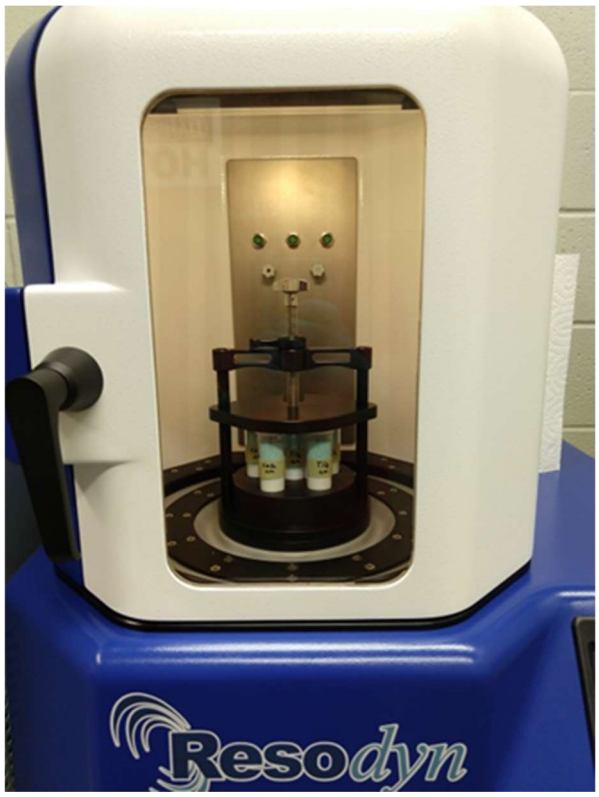

Figure 1 The LAB RAM II Resodyn Resonant Acoustic Mixer used to mix all formulations herein.

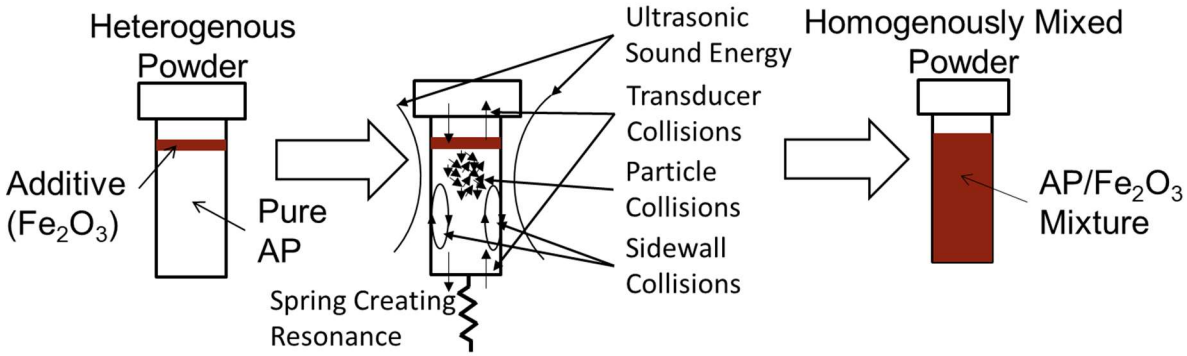

Figure 2 Schematic of mixing and forced used to create the homogeneous mixture of AP/additive.

3.3 Sample Preparation

Once a homogenous mixture of AP and catalyst was achieved, the pellet formulations needed to be completed. The first step to form an AP pellet is to clean the custom pellet punch assembly. A cutaway of the pellet punch which consisted of an anvil (bottom piece), a die (the center cylindrical piece), and the punch (the long piece that applies the force on to the material), shows best the details. All these components can be seen in a SolidWorks cutaway view in Fig. 3.

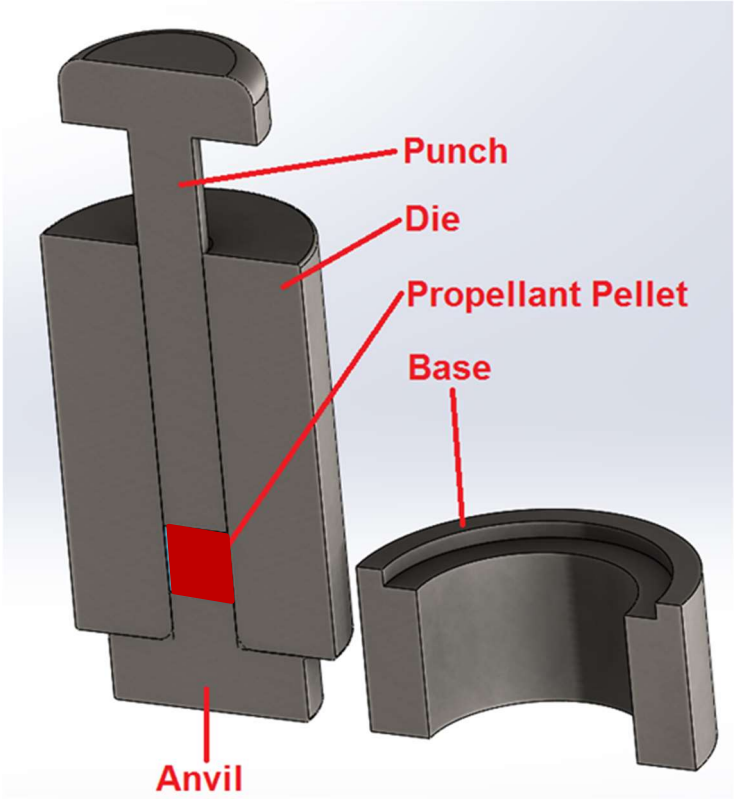

Figure 3 Computer-generated pellet punch cutaway showing how a powdered propellant is pressed into a pellet.

The pellet punch assembly was made from A10 tool steel. This material was chosen due to easy machinability and its high metal-on-metal wear resistance. Prior to use, all pieces of the assembly were heat treated to reduce the potential for localized plastic deformation during pressing. The heat treatment process consisted of heating all pieces of the pellet punch assembly in a furnace to 650℃ at a ramp rate of 1℃ per minute and holding at that temperature for two hours, then the temperature was increased to 810℃ at a ramp rate of 10℃ per minute and held for one hour. Lastly, the assembly was allowed to air cool to room temperature [26]. The various pellet punch components before and after heat treatment can be seen in Fig. 4.

Figure 4 (top) Pellet punch assembly prior to heat treatment. (bottom) Pellet punch assembly after heat treatment.

A PTFE dry film lubricant was applied to the inside of the pellet punch assembly before any material was placed inside. The appropriate amount of material per Table 2 was placed inside of the pellet punch and loaded into a Carver M-NE3890 hydraulic press. This press is programmable and has the capability of achieving a clamping force of 50,000 lb_f. The parameters used to compact the material were 12,000 lb_f for one hour.

Figure 5 (left) Carver M-NE3890 programmable hydraulic press. (right) Pellet punch assembly loaded into the Carver hydraulic press.

Due to the crystalline structure of the AP a long pressing time was needed to surpass the desired density threshold. The achieved densities are detailed in Table 1. When the pressing cycle was completed, the anvil was taken out and the die was placed

on top of a base and placed back into the press. A force was reapplied to carefully push the pellet out of the die. The Carver M-NE3890 hydraulic press and loaded pellet punch assembly can be seen in Fig. 5. A schematic of how the hydraulic press compacts the homogenous mixture is shown in Fig. 6.

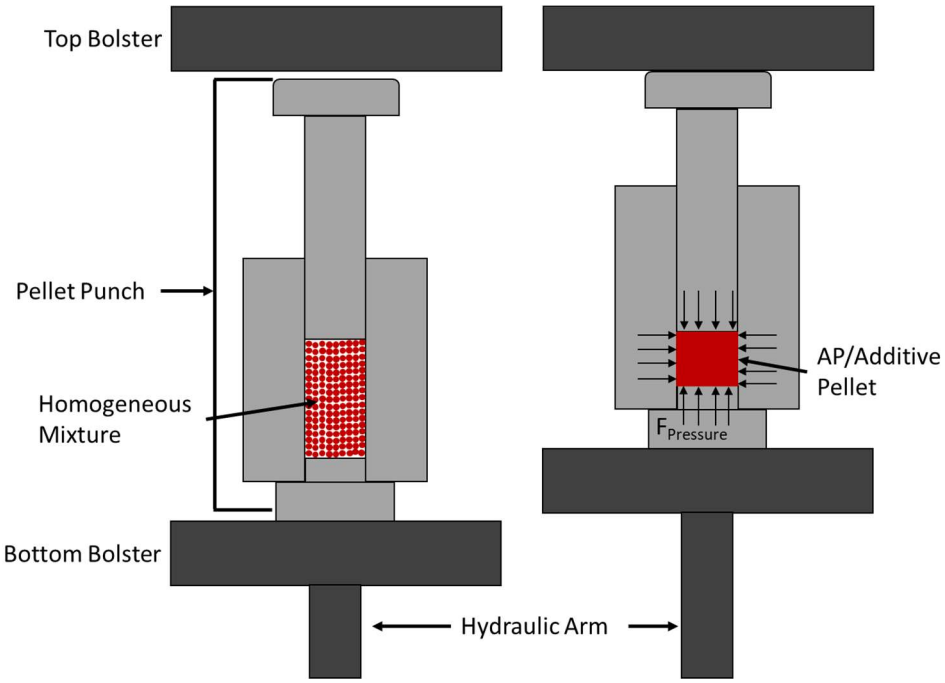

Figure 6 (left) Pellet punch with uncompressed mixture. (right) Force applied through the extension of the hydraulic arm to compact the mixture and create a pellet.

3.4 Strand Burner and Data Acquisition

The ballistic testing was conducted in a constant-volume strand burner which has the capability of testing up to 55.2 MPa (8,000 psi); for the experiments conducted herein, formulations were tested up to 34.5 MPa (5,000 psi). The strand burner has four

optical ports that can be utilized to perform various diagnostics and alter the ignition methods. The three optical ports located on the sides of the strand burner allow for various diagnostics such as mass spectroscopy, high-speed video, and photoreceiver light emission. Another optical port is located on the top of the strand burner and allows the capability for CO_2 laser ignition (not used herein). The locations of all optical ports

are shown in Fig. 9. The constant-volume stand burner utilized herein is shown in Fig. 7. The strand burner design is discussed in more detail by Carro et al. [27,28].

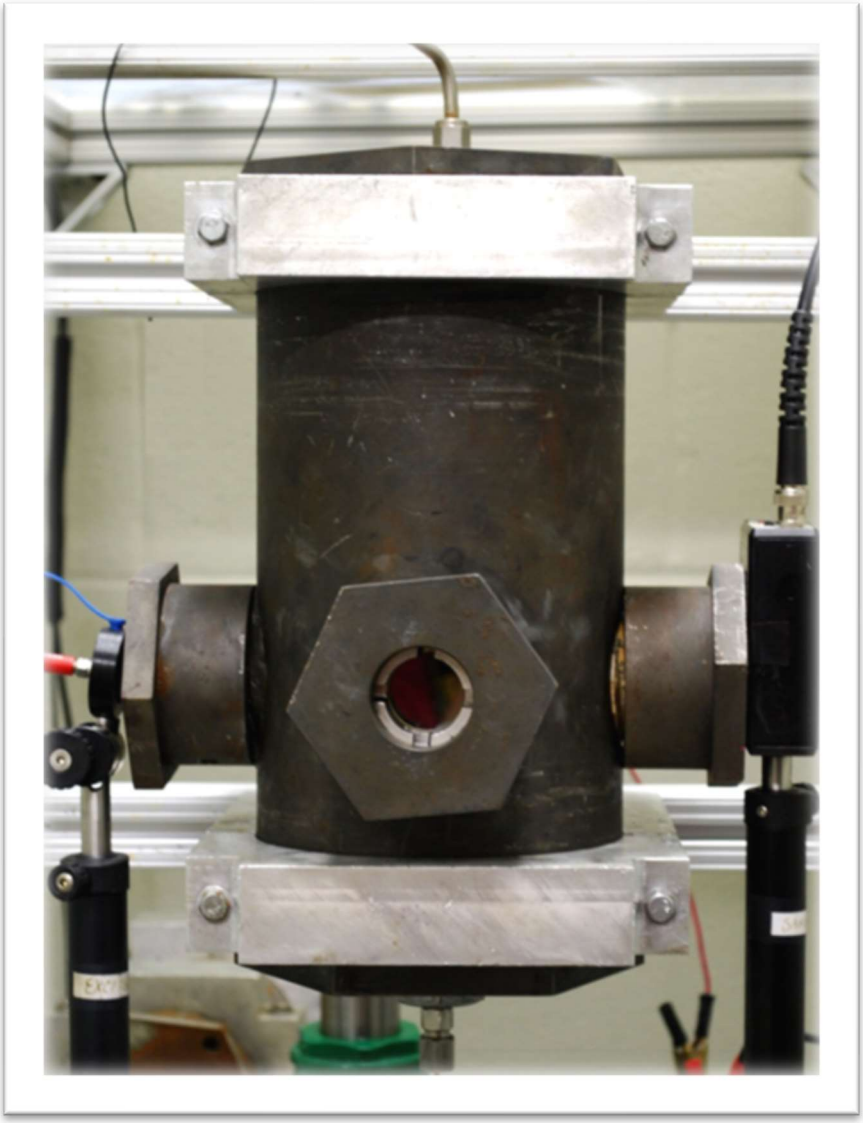

Figure 7 High-pressure, constant-volume strand burner utilized herein.

A modified stainless-steel bolt equipped with a Conax copper ignition lead wire and Viton O-ring served as a custom sample holder. The sample holder screwed into the bottom of the strand burner and sealed using a replaceable O-ring. The custom sample holder can be seen in Fig. 8. This method for mounting samples is based on the techniques used over the past several years in the Petersen laboratory [2-15,20,25,27-29]. A cutaway of the strand burner showing how the custom sample holder is mounted can be seen in Fig. 9.

Figure 8 Custom sample holder used to load samples into the test vessel.

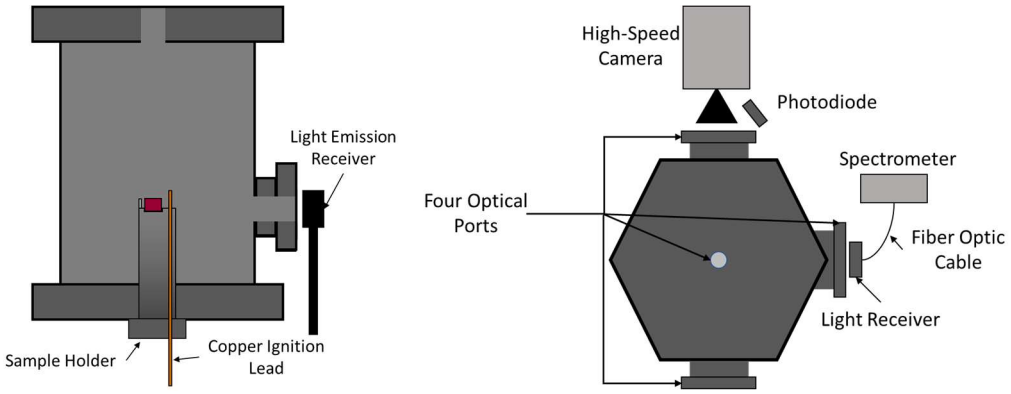

Figure 9 (left) Cutaway view of the strand burner showing the sample holder. (right) Location of optical ports and supporting diagnostics.

Prior to loading the sample for ballistic testing, a quarter inch-wide piece of tape was attached around the circumference of the uninhibited face of the pellet, a razor blade was then used to create two slits opposite of each other. The sample was then placed inside of a slot located at the top of the sample holder. A nichrome wire was attached to the ignition and ground leads and put in contact with the uninhibited face of the pellet. Approximately 0.15g of igniter material (Boron potassium nitrate, $BKNO_3$) was weighed and spread out in an even coat over the uninhibited face of the pellet and nichrome wire. Lastly, a piece of tape was placed over the igniter material to reduce the possibility of the igniter material getting displaced during the pressurizing procedure. These

procedures are based on those originally shown in the thesis by Tykol [25]. Figure 10 shows the steps taken to prepare the samples prior to ballistic testing.

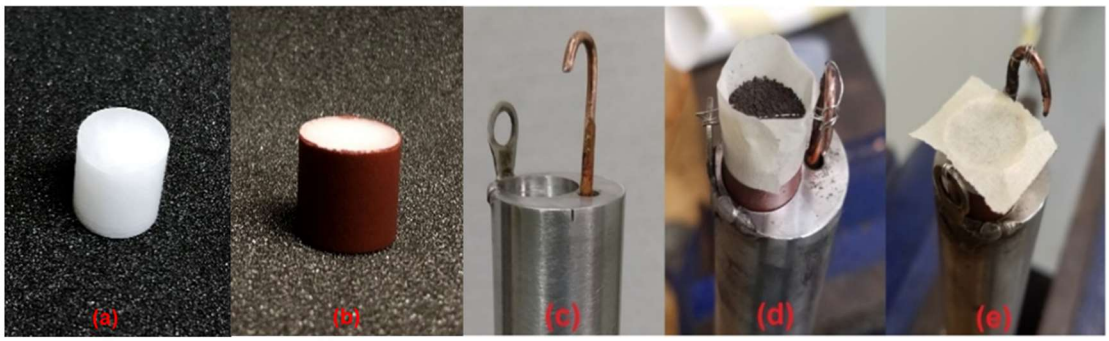

Figure 10 Sample loading process. A sample (a) was inhibited (b) and placed on the custom sample holder (c) slits were cut for the nichrome wire, a piece of nichrome wire was connected across the leads, and $BKNO_3$ was loaded (d). Lastly, tape was pressed over the top to secure the powder (e)

The custom sample holder was then screwed into the strand burner until solid contact between the O-ring and bottom face of the strand burner was realized. Ignition was achieved by running 18 volts and 7.5 amps through the nichrome wire. The $BKNO_3$ is a highly sensitive material and combusts immediately once an electric current is applied. The rapid combustion creates a uniform flame on the surface of the pellet. The one-dimensional propagation of the flame front can be corroborated using the high-speed video. The transient combustion phenomena are monitored by a pressure transducer (OmegaDyne PX02C1-7.5KG), light emission diode (New Focus 2031), UV-VIS

spectrometer (Ocean Optics USB2000), and high-speed video (Photron FASTCAM SA3 120K). A schematic of the test setup can be seen in Fig. 11.

Once the custom sample holder is secured in the strand burner, safety checks were completed and the data acquisition (DAQ) system was prepared. The test cell utilized at the Turbomachinery Laboratory has steel-reinforced concrete walls and a blast-proof door. A separate control room contains the DAQ systems and control board used to remotely pressurize and ignite the sample. The vessel is pressurized using nitrogen, an inert gas, and three pressure transducers track all changes in pressure. One of the transducers was used for GageScope, this program records voltage signals from the Gage Applied Sciences DAQ board. The other two transducers were used to output the pressure readings on the control board. One of the transducers was used solely for calibration and was never exposed to combustion or exhaust gasses.

Two pneumatic valves were used to control the flow of nitrogen to and from the test vessel. The transient combustion phenomena are monitored by a pressure transducer (OmegaDyne PX02C1-7.5KG), light emission diode (New Focus 2031), UV-VIS spectrometer (Ocean Optics USB2000), and high-speed video (Photron FASTCAM SA3

120K). All the data was collected and saved remotely in the control room. Further information on the test facility can be found in papers by Carro et al. [27,28].

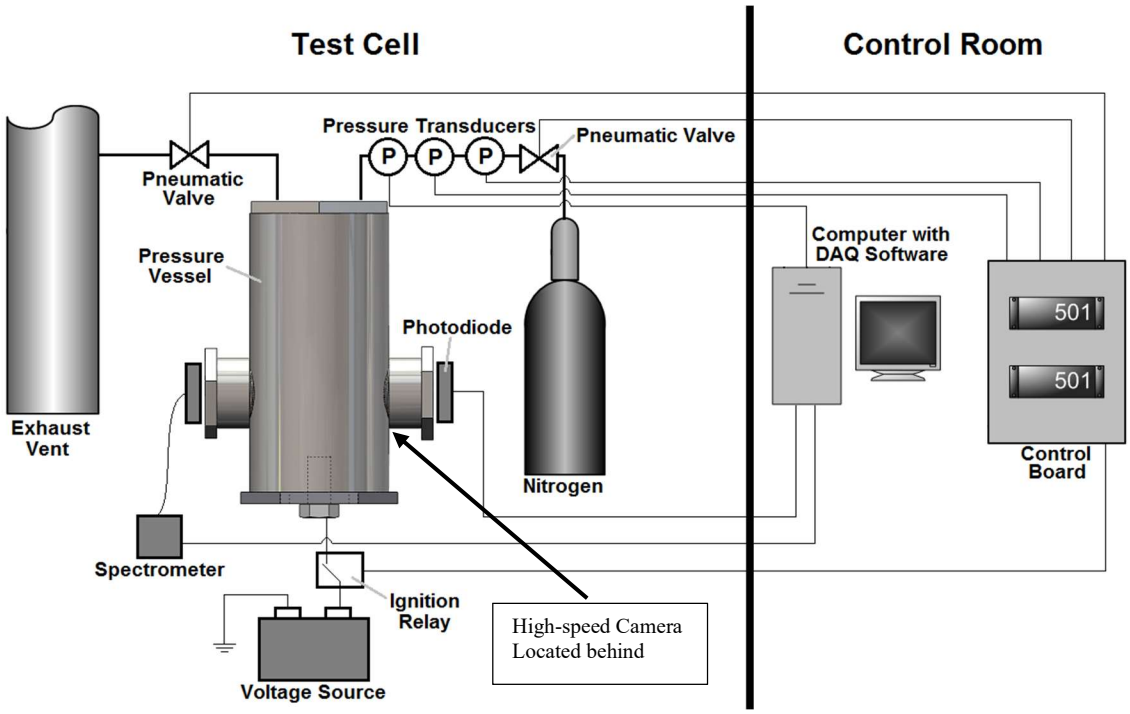

Figure 11 Test facility experimental setup. High-speed camera (not shown) located behind pressure vessel and connects to computer.

Ballistic testing was completed, and data were recorded for all formulations. Each formulation was tested over a pressure range of 3.45 MPa (500 psi) to 34.5 MPa (5,000 psi). Ten samples were burned for all formulations, and several formulations were retested to ensure repeatability.

4. RESULTS AND DATA ANALYSIS*

4.1 Material Characterization

Scanning Electron Microscopy (SEM) images of the micro-particle additives were taken on a Tescan VEGA3 SEM to evaluate fundamental particle sizes. SEM samples were prepared by scattering additive particles on the surface of a carbon film atop an aluminum pedestal. Representative images of the μTiO_2 and μFe_2O_3 and particles are shown in Figs. 12 and 13, respectively. The manufacturer of the micro-TiO_2 additive (Millapore Sigma) indicates a 325-mesh size (i.e. < 44 μm). The collected SEM images illustrate a wide range of particle sizes from approximately 10-50 μm and a rough surface topology. The manufacturer indicates the oxidation state of the additive as titanium (IV) oxide (i.e. TiO_2) with a crystal structure that is > 99% anatase. The manufacturer of the μFe_2O_3 additive (Firefox Enterprises) indicates a 325-mesh size (i.e. < 44 μm). The collected SEM images illustrate a wide range of particle sizes from approximately 1-50 μm and a rough surface topology. The manufacturer only indicates an oxidation state of the additive as iron (III) oxide (i.e. Fe_2O_3), and does not include information regarding the crystal structure (i.e. α- Fe_2O_3, γ- Fe_2O_3, etc.).

* Parts of this section is reprinted from "Burning Rate Characterization of Ammonium Perchlorate Pellets Containing Catalytic Additives" with permission from Rodriguez, F. A., AIAA 2019-4440, 2019 AIAA Joint Propulsion Conference, Indianapolis, IN, 2019, and from "Burning Rate Characterization of Ammonium Perchlorate Pellets Containing Nano-Catalytic Additives" with permission from Rodriguez, F. A., AIAA 2020-1425, 2020 AIAA Science and Technology Conference, Orlando, FL, 2020.

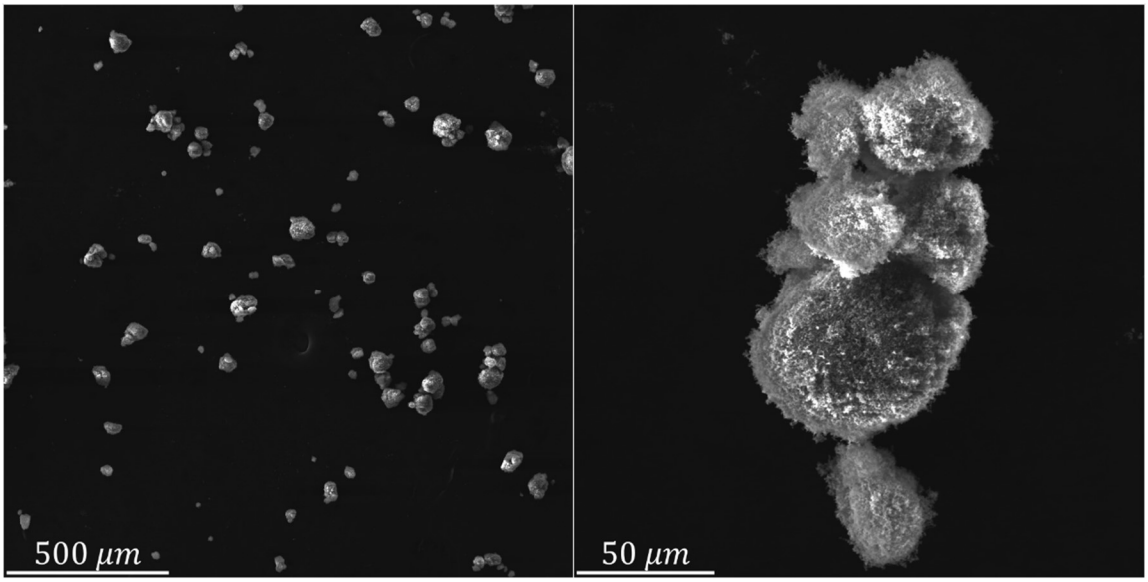

Figure 12 SEM images of µTiO_2 particles. (left) Several particles at a magnification of 100× and (right) a particle agglomerate at a magnification of 850×.

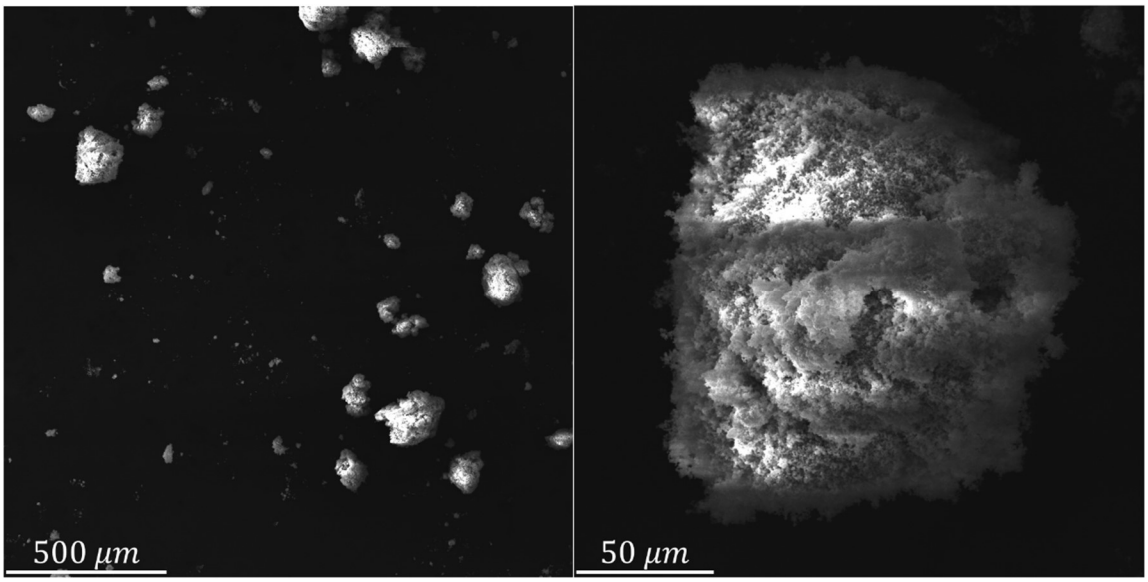

Figure 13 SEM images of µFe_2O_3 particles. (left) Several particles at a magnification of 100× and (right) a single particle at a magnification of 850×.

Transmission Electron Microscopy (TEM) images of the nano-particle additives were taken on a JEOL 1200 EX TEM to evaluate their fundamental particle sizes. TEM samples were prepared by dispersing additive particles in an aqueous solution of methanol solvent at a mass concentration of 5% and subjecting the mixture to a 15-minute ultra-sonication treatment. The samples were diluted in a 5:1 volumetric ratio with additional solvent and suspended on a carbon-film, 400-mesh copper grid. The solvent was evaporated off the grid at atmospheric conditions. TEM images were taken at various magnifications, and representative images of $nTiO_2$ and nFe_2O_3 are shown in the left and right images of Fig. 14, respectively. The specifications given by the manufacturer of the nano-additives evaluated herein (Mach I Chemicals, Inc.) are given in Table 3. The TEM images indicate fundamental particle sizes of approximately 20 and 5 nm for the $nTiO_2$ and nFe_2O_3, respectively, which is in good agreement with the manufacturer-provided specifications. The manufacturer indicates a 70/30 ratio of anatase/rutile crystal structure in the TiO_2 nano-additive and amorphous structure (no crystalline order) in the Fe_2O_3 nano-additive. The oxidization states of the nano-additives are the same as for the analogous micro-additives. It is worth noting the appearance of 'lighter' spots in the $nTiO_2$ image indicates some level of porosity in the additive.

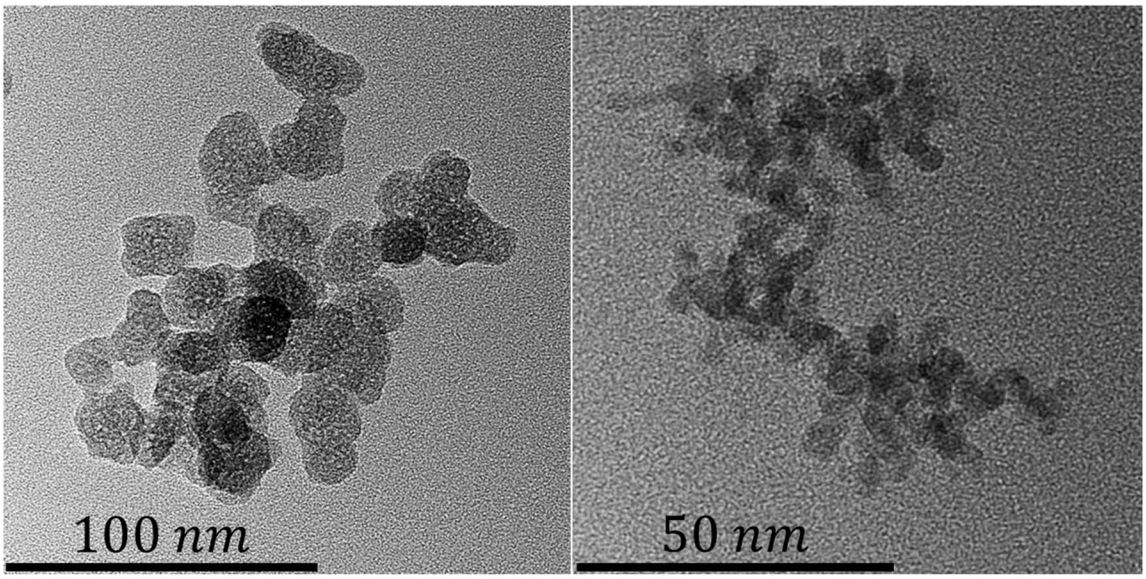

Figure 14 Representative TEM images of (left) $nTiO_2$ at a magnification of 100k× and (right) nFe_2O_3 at a magnification of 200k×.

Table 3 Nano-additive specifications provided by the manufacturer.

Additive	$nTiO_2$	nFe_2O_3
Color	White	Reddish Brown
Structure	70%/30% Anatase/Rutile	Amorphous
Shape	Spherical	Spherical
Purity	> 95%	99.3
Particle Size (nm)*	15-20	3-5
Surface Area (m^2/g)*	96	269

*Batch-Specific, Manufactured-Measured Parameter

SEM images of the representative AP pellets containing micro- and nano-additives were taken on a Tescan VEGA3 SEM to evaluate the dispersion and homogeneity of these additive within the system. Representative SEM images of AP pellets containing 1% μTiO_2 and μFe_2O_3 are shown in Figs. 15 and 16, respectively. Part (a) of these figures shows the entirety of the AP pellet sample and demonstrate the lack of any macro-scale porosity or inconsistencies. Parts (b) and (e) of these figures show back-scatter SEM (BSE) images of the pellet surface at low-level (50×) and high-level (250×) magnification, respectively. The lighter elements (i.e. Ti or Fe) appear lighter in BSE images and can be utilized to trace additives in the system. Parts (c-d) and (f-g) of these images show Energy Dispersive Spectroscopy (EDS) maps of the pellet surface at low-level (50×) and high-level (250×) magnification, respectively. Individual elements are traced and mapped to the propellant surface. The presence of AP is mapped with chlorine ([Cl], red), and the presence of either additive is mapped by its corresponding metal ([Ti] or [Fe], blue). In general, the micro-additives are well-dispersed throughout the pellet and are not significantly agglomerated. Furthermore, the BSE and EDS images show good agreement in terms of additive particle location, demonstrating the utility of either method for future characterization purposes.

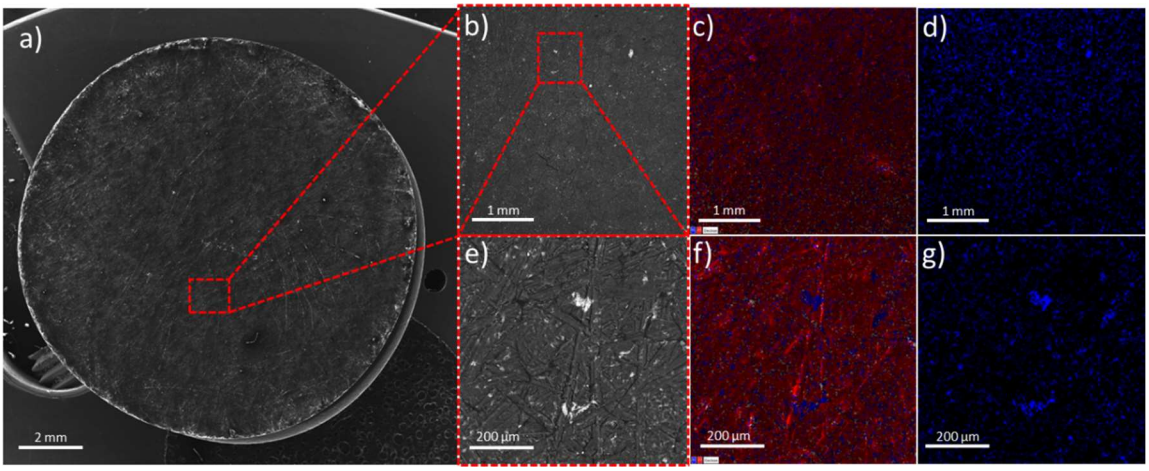

Figure 15 SEM imaging of an AP pellet containing 1% μTiO_2. a) Plain, wide-view SEM image of the entire pellet at a magnification of 15×. b-d) 50× magnification views of the pellet surface. b) back-scatter image, c) EDS overlay with (red) chlorine and (blue) titanium, and d) EDS overlay of only titanium. e-g) 250× magnification views of the pellet surface. e) back-scatter image, f) EDS overlay with (red) chlorine and (blue) titanium, and g) EDS overlay of only titanium.

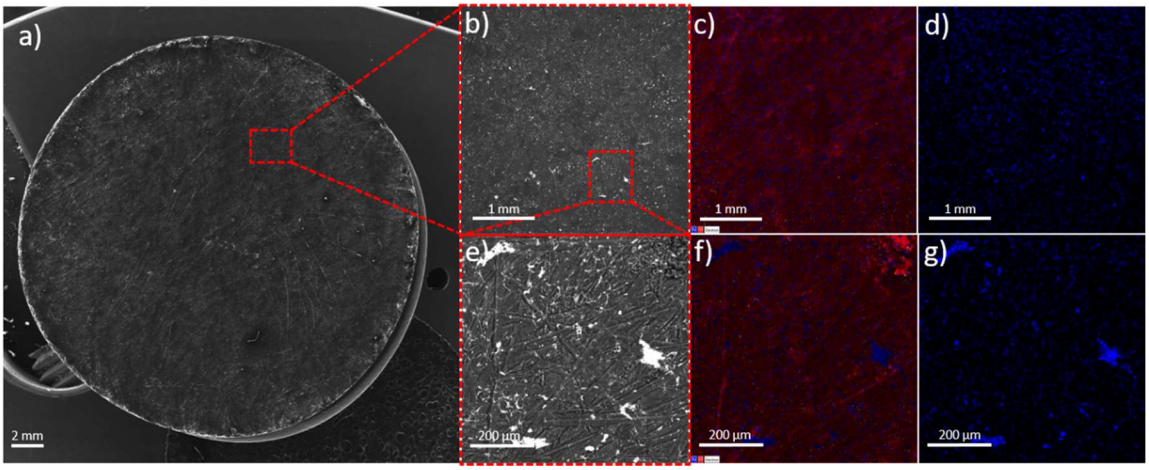

Figure 16 SEM imaging of an AP pellet containing 1% μFe_2O_3. a) Plain, wide-view SEM image of the entire pellet at magnification of 15×. b-d) 50× magnification views of the pellet surface. b) back-scatter image, c) EDS overlay with (red) chlorine and (blue) iron, and d) EDS overlay of only iron. e-g) 250× magnification views of the pellet surface. e) back-scatter image, f) EDS overlay with (red) chlorine and (blue) iron, and g) EDS overlay of only iron.

Representative BSE images of AP pellets containing 1% $nTiO_2$ and nFe_2O_3 are shown in Figs. 17 and 18, respectively. The left, middle, and right images of these figures correspond to increasing magnifications of 100×, 500×, and 1.5k×, respectively. High-magnification (1.5k×) images show the presence of some micro-scale agglomerates of the nano-particles, but most of the additive is contained in aggregate systems of 1 μm or less. In comparison to BSE images of the AP pellets containing micro-additives (Figs. 15 and 16), there are significantly fewer visible additive particles in the BSE images of pellets containing nano-additives (Figs. 17 and 18). This observation is possibly related to the resolution of the SEM (~25 nm) which is larger than the fundamental nano-particles, so that non-agglomerated nano-particles would not be readily visible in the BSE images of Figs. 17 and 18. These findings suggest that the nano-particles are well dispersed throughout the AP pellet and are not significantly agglomerated.

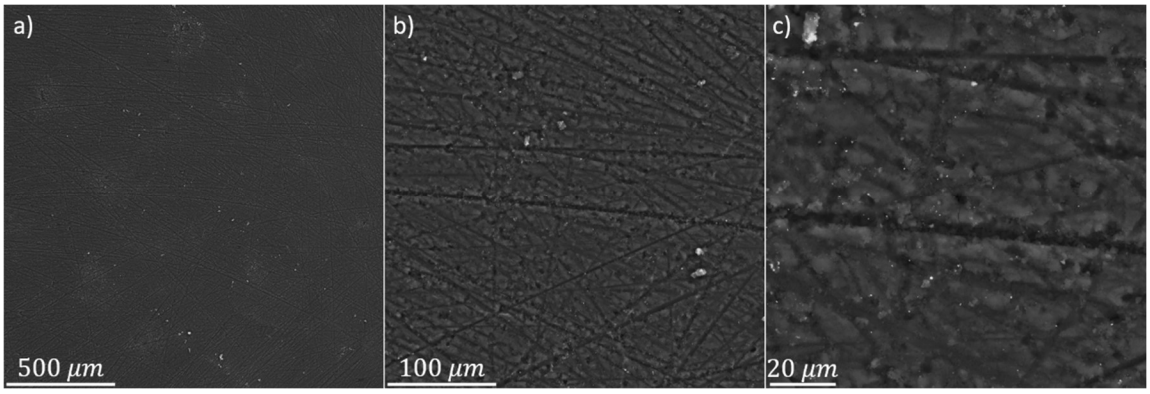

Figure 17 Back-scatter SEM images of an AP Pellet containing 1% $nTiO_2$ at magnifications of a) 100×, b) 500×, and c) 1.5k×.

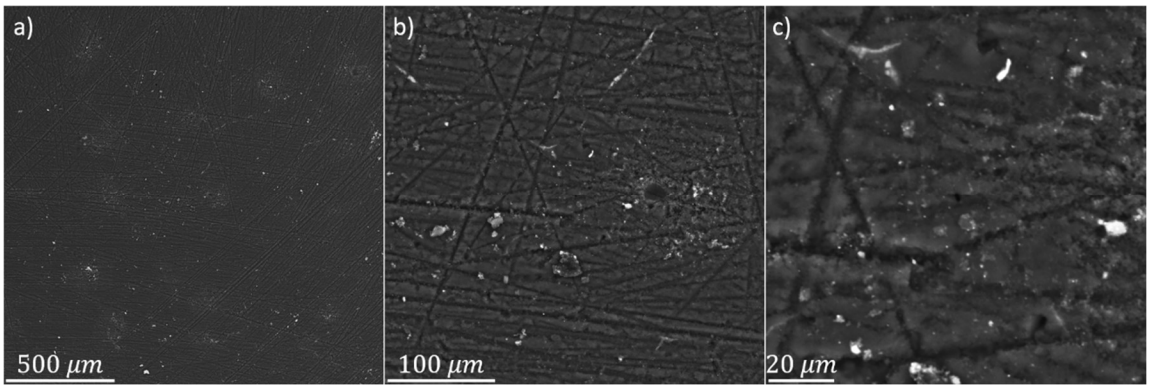

Figure 18 Back-scatter SEM images of an AP Pellet containing 1% nFe_2O_3 at magnifications of a) 100×, b) 500×, and c) 1.5k×.

4.2 Burning Rates

The sample length and burn times were the two crucial values needed to calculate the burning rate of a propellant sample. With these two values, the burning rate could be calculated by simply dividing sample length by burn time as seen in Eqn. 1.

$$\boldsymbol{r = \frac{l}{\Delta t}} \quad \textbf{(1)}$$

The length of the pellet was measured using digital calipers after the pressing process, but burn time needed to be experimentally determined. The strand burner is equipped with several tools to collect data that can be used determine the beginning and end times of the combustion process. Examples of the data collected that can be used to extrapolate burn time are: pressure trace, light trace, and high-speed video. The pressure trace is most commonly used in the author's laboratory to determine the burn time, although all three methods have been proven to agree. An example of how burn time can be extracted from pressure and light traces can be seen in Fig. 19.

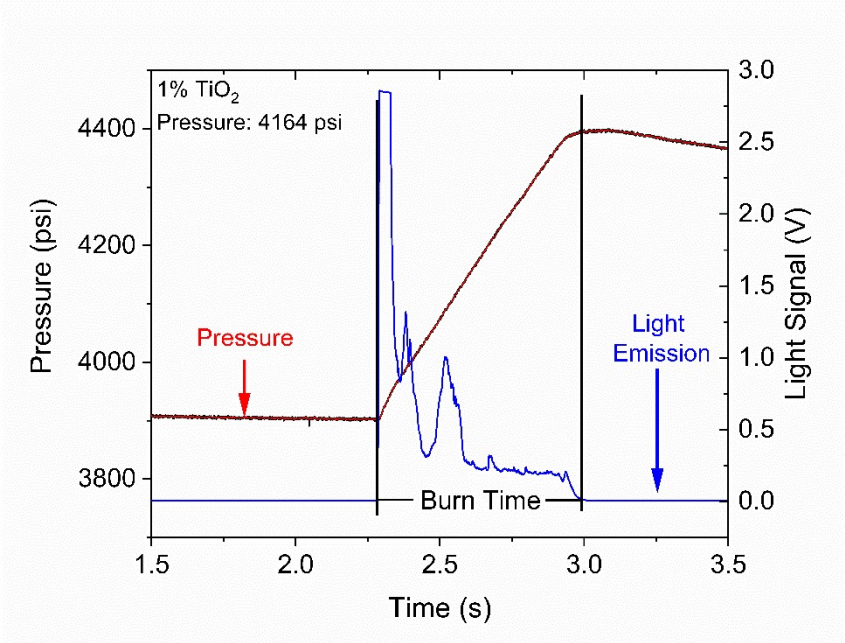

Figure 19 Example data reduction for burn time from pressure and light trace.

The pressure and light traces show sharp slope increases when combustion begins allowing the burn start time to be determined easily. This sharp increase in the pressure and light trace is attributed to the $BKNO_3$ combusting rapidly. A uniform flame is immediately propagated on the top surface of the pellet. This uniform flame translates to a one-dimensional burning profile than can be corroborated using the high-speed camera. The high-speed video displays the burn start time with a flash of light in a similar way as the light emission trace.

The burn end time can be determined from the pressure trace as the end of the linear increase in pressure. The pressure trace is normally used to determine the start and end time of the burn, and the other two methods are used to decipher any anomalous trends that are seen in the pressure trace.

Once all sample lengths and burn times were collected, burning rates were correlated using Eqn. 1. Burning rate curves with pressure on the x-axis and burning rate on the y-axis with a log-log scale were constructed for each formulation. The ballistic testing data are displayed and discussed in the next section.

4.3 Ballistic Testing Data

A baseline ballistic dataset for plain AP without any additives and specific to the author's test facility has been collected and presented by Petersen et al. [29]. Several, different-sized pellets and pressing parameters (force and time) were explored, along with various ignition methods before the method outlined in the experimental procedure section above was carefully chosen. This method was selected due to production of high pellet densities and maximum reproducibility of burning rate data. The baseline data along with literature data compiled by Petersen et al. [29] can be seen in Fig. 20.

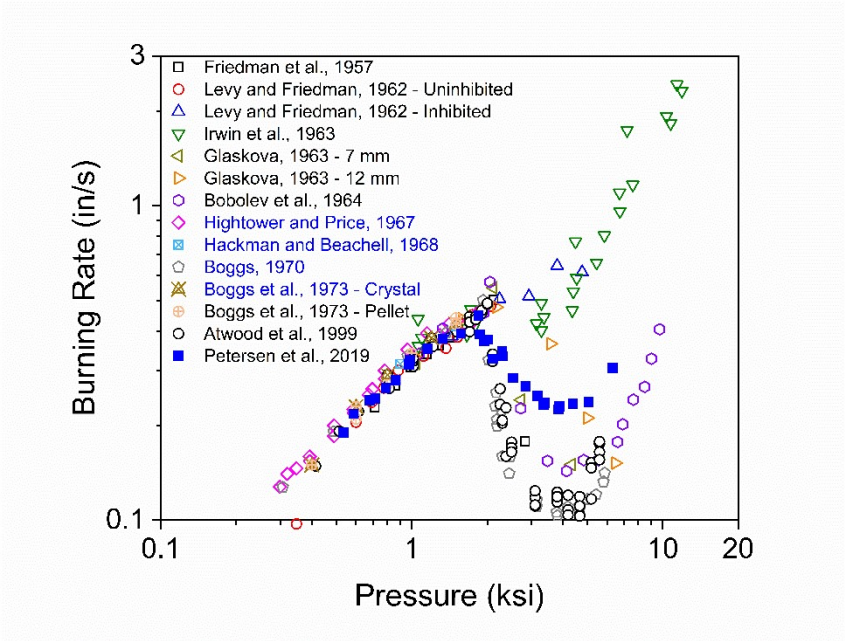

Figure 20 TAMU plain AP baseline with compiled baseline data from other facilities.

Once the baseline dataset was fully constructed, pellets with μTiO_2 and μFe_2O_3 were evaluated. The loading percentage of the catalysts were initially varied from 1 to 3%. An additional, 0.5% μFe_2O_3 formulation was tested to investigate the existence of a catalytic loading and performance threshold. All of the burning rate data collected herein for AP formulations containing μTiO_2 or μFe_2O_3 are shown in Fig. 21, along with the corresponding plain AP baseline. The data for formulations containing μTiO_2 and μFe_2O_3 are separated in the left and right plots of Fig. 22, respectively, and trend lines are drawn to highlight key trends.

In general, the formulations containing μTiO_2 yielded a reduction in the burning rates at lower pressures (< 2,000 psi), but were effective at increasing the burning rate at higher pressures. Furthermore, the formulation containing the least amount of catalyst

(1%) exhibited the highest burning rates among the formulations containing μTiO_2. It is worth noting that the AP formulation containing 1% μTiO_2 was manufactured and tested twice to establish repeatability.

In general, the formulations containing μFe_2O_3 yielded an increase in burning rate across all of the pressures evaluated herein and were more effective at higher pressures. Similar to the trends observed for formulations containing μTiO_2, the performance of the propellant decreased as the catalyst loading was incrementally increased from 1% to 3%.

An additional 0.5% μFe_2O_3 formulation was tested to investigate the existence of a catalytic loading and performance threshold. This formulation deviated from the expected trend. In comparison to the formulation containing 1% μFe_2O_3, the burning rate was slightly higher at higher pressures (> 3,000 psi), and the catalytic effect decreased more rapidly at lower pressures.

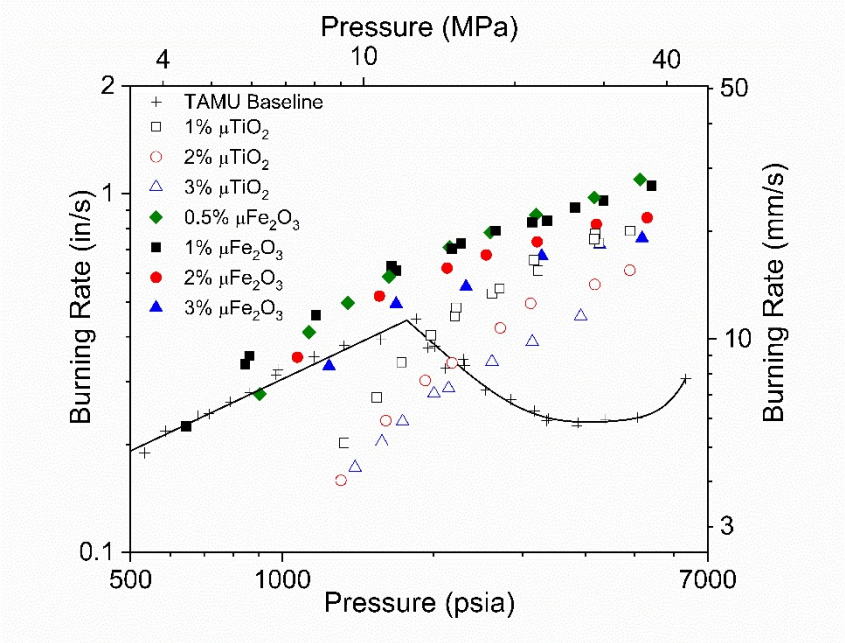

Figure 21 Burning rate data for plain AP pellets and AP pellet formulations loaded with 0.5, 1, 2 and 3% μFe_2O_3 and 1, 2 and 3% μTiO_2.

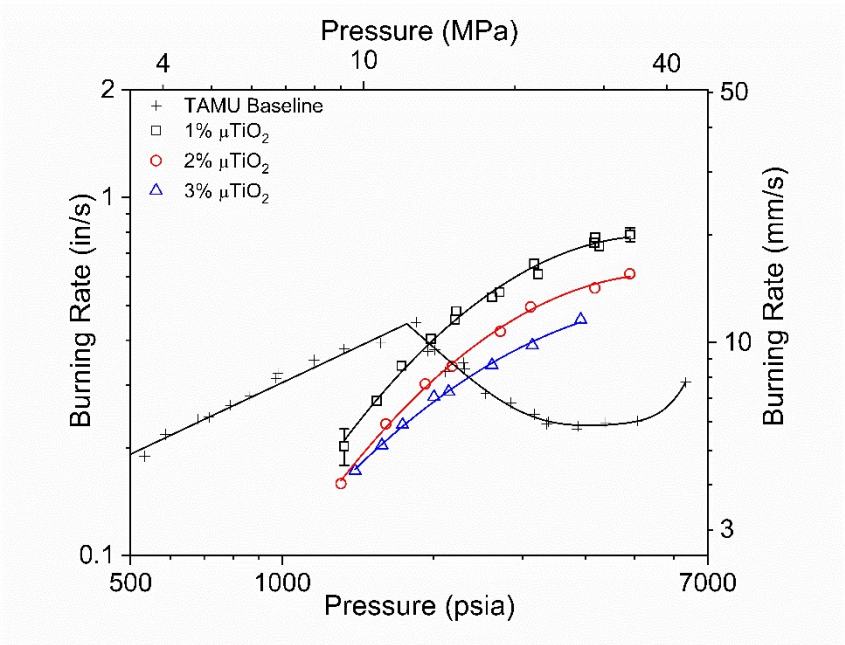

Figure 22 Burning rate data for plain AP pellets and pellet formulations loaded with 1, 2 and 3% μTiO_2 with overlaid observed trend lines.

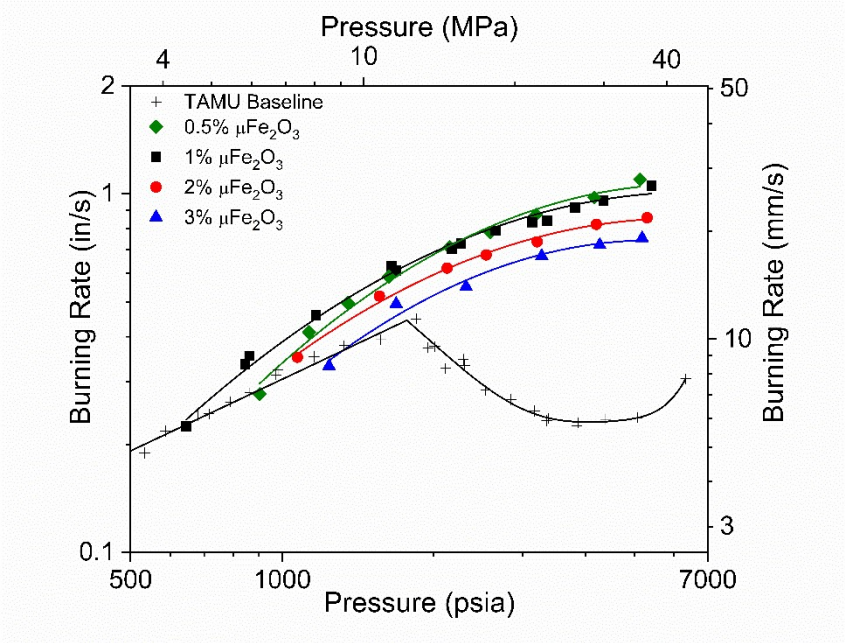

Figure 23 Burning rate data for plain AP pellets and pellet formulations loaded with 0.5, 1, 2, and 3% μFe_2O_3 formulations with overlaid trend lines.

Implementation of μTiO_2 in AP pellets has not been documented in the open literature, so no comparison of the trends observed herein can be made to previous studies. However, previous studies have been conducted with AP/μFe_2O_3 pellets. The available literature data [21-23] have been compiled and are compared to the current dataset in Fig. 24. The left plot of Fig. 24 compares data for 2% and 3% μFe_2O_3 formulations taken from Boggs et al. [22] and Friedman et al. [21], respectively, with the current dataset. There is good agreement between the current dataset and the data presented by Friedman et al. [21] in terms of general trends and quantitative pellet burning rates. However, there is poor agreement between the data presented by Boggs et al. [22] and the other available data. More explicitly, the data given by Boggs et al. [22] suggest μFe_2O_3 is an effective catalyst in the lower-pressure regime, which is in discord

with the current dataset and the data presented by Friedman et al. [21]. These observations indicate that the effects of the μFe_2O_3 additive on the combustion behavior of AP are dependent on the specific additive characteristics, such as size and geometry, rather than just the chemical composition (i.e., Fe_2O_3). This finding is further supported by the observations made by Marothiya et al. [23] where utilization of μFe_2O_3 from various sources led to significant changes in the catalyst effectiveness in AP pellets. Accordingly, the present author suggests that in all future ballistic studies involving solid propellant ingredients with catalytic additives, that the catalysts be well characterized in terms of their chemical composition, particle size, geometry, and surface characteristics.

Data for mechanically mixed 0.75-3% μFe_2O_3 formulations from Marothiya et al. [23] are compared with the current dataset in Fig. 25. Once again, there is good agreement between the two datasets in terms of general trends and quantitative burning rates. Furthermore, the pellet burning rates in both datasets increase with increasing catalyst concentration, and then decrease upon further loading (> 1%). These observations suggest that an optimal catalyst concentration exists for any given catalyst/propellant combination. This trend is related to competing effects during the combustion of catalyst-loaded AP samples. The metal oxides provide a catalytic mechanism that, at most pressures, serves to increase the burning rate of the AP. However, the metal oxides do not react during the combustion process since their melting and vaporization points are higher than the adiabatic flame temperature of the reaction. The metal oxides therefore also soak heat away from the reaction which reduces the flame temperature. The relative dominance of each of these two effects

yields an optimal catalyst concentration for maximum burning rate performance, which is dependent on the specific catalytic additive utilized.

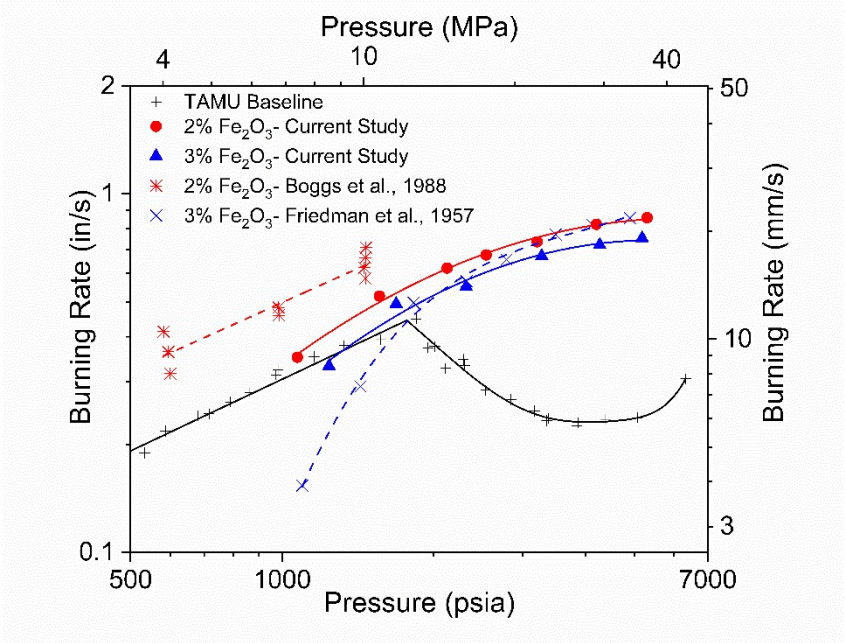

Figure 24 Comparison of literature burning rate data for AP pellets containing μFe_2O_3 to those data collected in the current study. Data from Boggs et al. [22] for AP with 2% μFe_2O_3 and Friedman et al. [21] for AP with 3% μFe_2O_3.

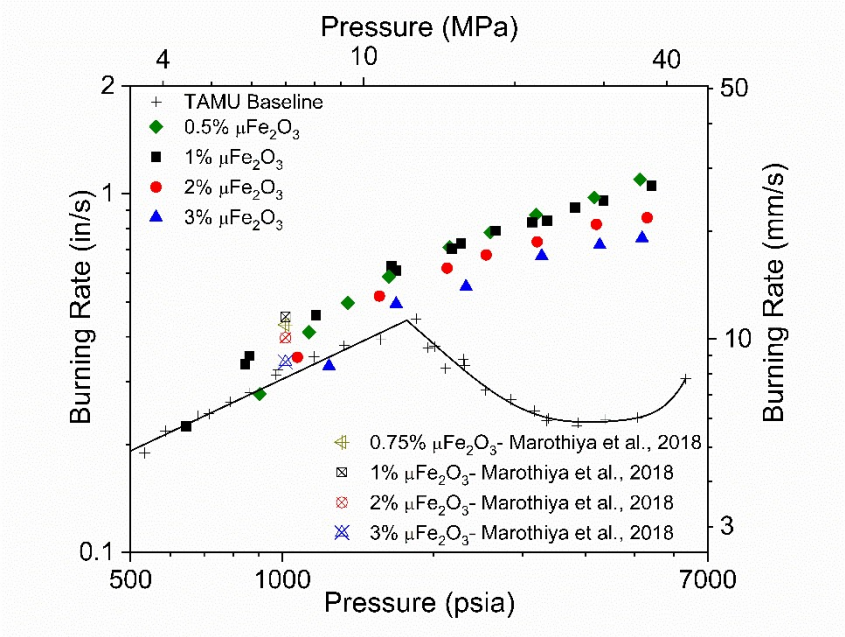

Figure 25 Comparison of literature burning rate data for AP pellets containing μFe_2O_3 to those data collected in the current study. Data from Marothiya et al. [23] for 0.75-3% μFe_2O_3 mechanically mixed with AP.

All of the burning rate data collected herein for AP formulations containing $nTiO_2$ and nFe_2O_3 are shown in Fig. 26, along with the corresponding plain AP baseline. The data for formulations containing $nTiO_2$ and nFe_2O_3 are separated in Figs. 27 and 28, respectively, and trend lines are drawn to highlight key trends. In general, the catalytic effects of each additive were greater at 11.72 MPa and 8.27 MPa for the $nTiO_2$ and nFe_2O_3 formulations, respectively, in the region of depressed burning rates of plain AP—a well-established literature result. Furthermore, the formulations containing nFe_2O_3 yielded a higher increase in burning rate relative to the $nTiO_2$ formulations.

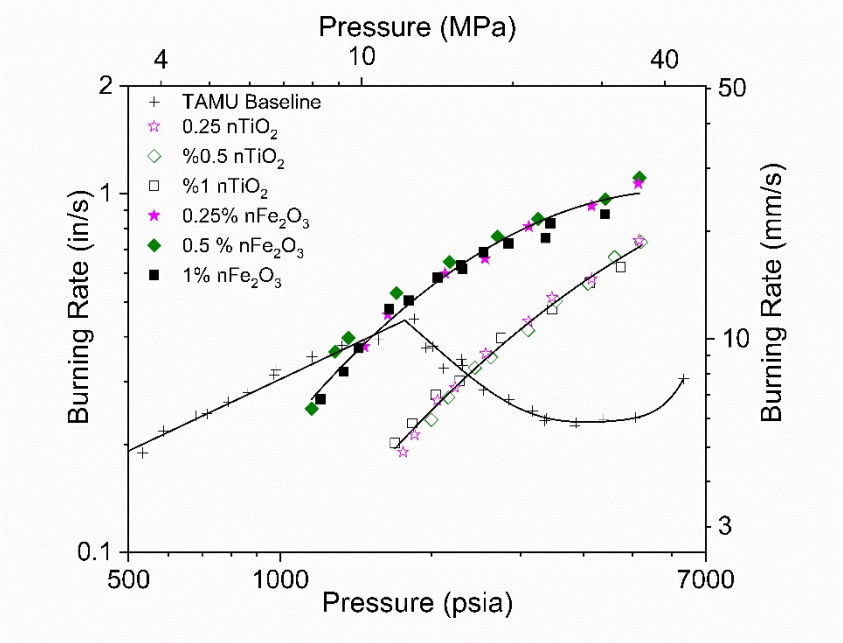

Figure 26 Burning rate data for plain AP pellets and AP pellet formulations loaded with 0.25, 0.5, and 1% nFe_2O_3 and 0.25, 0.5 and 1% $nTiO_2$.

The burning rate data for both nano- and micro-catalyst formulations are located in Figs. 29 and 30. To reiterate, the concentrations range from 0.5-3% and 0.25-1% for micro- and nano-formulations, respectively. Open symbols and dashed trendlines correspond to formulations containing micro-catalysts, while closed symbols and the solid black trendlines correspond to formulations containing nano-catalysts. The burning rates decreased as the concentration of micro-sized catalysts increased in the pellets. However, the same decrease in burning rate with an increase in catalyst concentration did not carry over when nano-forms of the catalysts were implemented, at least within the range of concentrations evaluated herein.

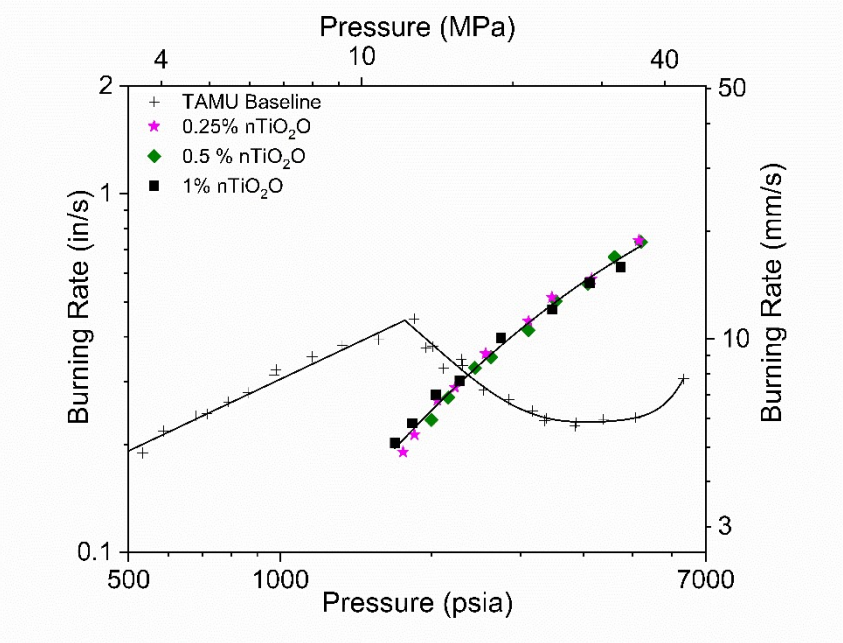

Figure 27 Burning rate data for plain AP pellets and pellet formulations loaded with 0.25, 0.5 and 1% $nTiO_2$.

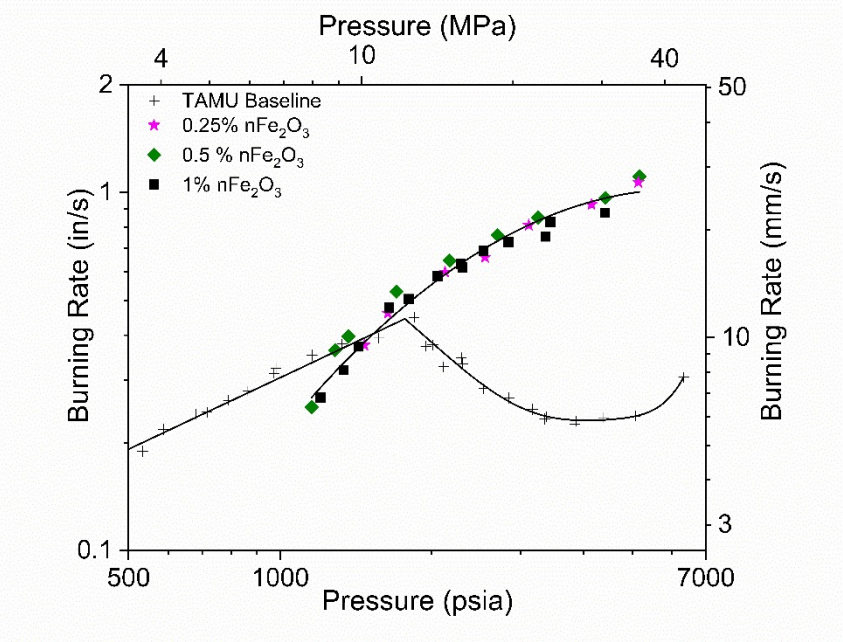

Figure 28 Burning rate data for plain AP pellets and pellet formulations loaded with 0.25, 0.5, 1% nFe_2O_3 formulations.

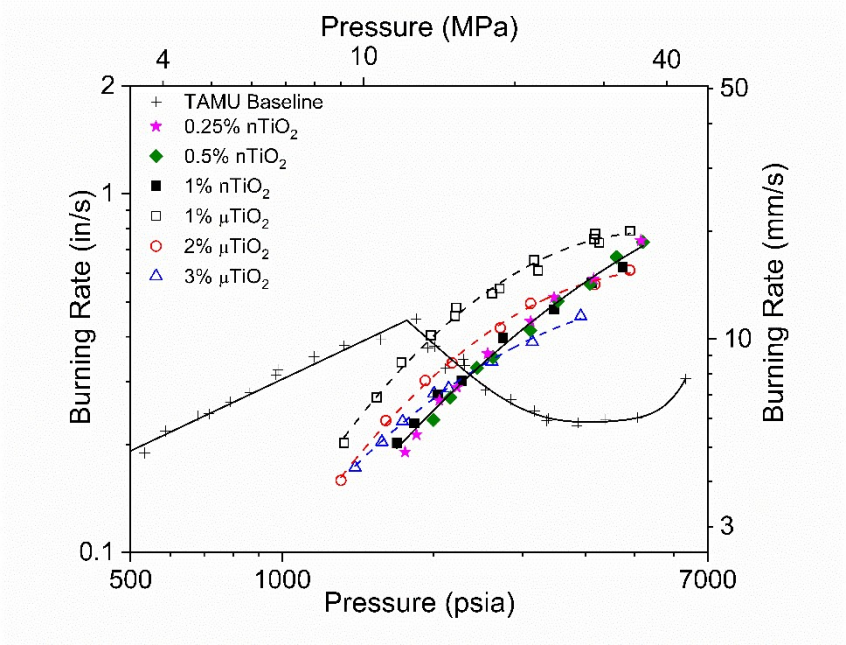

Figure 29 Comparison of burning rate data for μTiO_2 formulations with the $nTiO_2$ data.

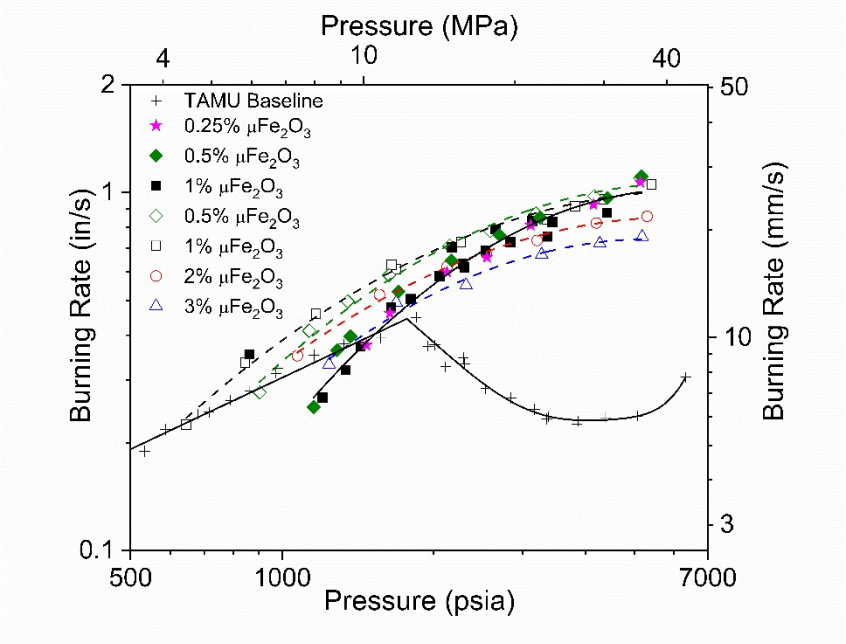

Figure 30 Comparison of burning rate data for μFe_2O_3 formulations with the nFe_2O_3 data.

The addition of $nTiO_2$ decreased the burning rates at lower pressures relative to the baseline and all μTiO_2 formulations, but displayed better burning rates than the 2 and 3% μTiO_2 formulations at higher pressures (2,500 psi). The nFe_2O_3 formulations exhibited a similar trend as the $nTiO_2$ formulations. More explicitly, the burning rates were lower than all the μFe_2O_3 formulations at lower pressures, and the effects of the catalyst increased the burning rates towards the burning rates seen by the 0.5 and 1% μFe_2O_3 formulations at higher pressures. The burning rates for all the nano-formulations considered in this study were lower than the 1% micro-formulations over the pressure range investigated. However, the burning rate data for all nano-formulations appear to trend higher at the higher pressures, and may outperform their micro-counterparts at higher pressures.

Additional parameters of importance for AP combustion are the deflagration limits. Testing efforts herein were not concentrated on an in-depth investigation of the lower or upper pressure deflagration limits (LPDL or UPDL) for the examined formulations, but some general trends can be extrapolated from the available data. Neither a LPDL nor an UPDL was established for the baseline, plain AP dataset by Petersen et al. [29] since the authors were able to successfully burn AP as a monopropellant within the entire experimental testing range investigated in that study (500-5,000 psi).

Testing at lower pressures proved difficult for all formulations containing metal oxide additives. Anomalous pressure traces were consistently collected in the lower-pressure regions (< 1,000 psi). Furthermore, pellet samples tended to quench during the

combustion process in the lower-pressure regions. Efforts were not made herein to fully characterize anomalous burning or quenched samples at the lower pressures. The minimum pressure at which anomalous burning occurred generally increased as the micro-catalyst concentration was increased, although the nano-catalysts did not exhibit the same trend, testing samples at lower pressures did still prove to be problematic. Anomalous pressure traces for the $nTiO_2$ and nFe_2O_3 formulations were collected in regions below 11.72 MPa (1,700 psi) and 8.27 MPa (1,200 psi), respectively. The minimum pressure at which anomalous burning occurred for formulations containing nano-catalysts was observed at higher pressures relative to similar formulations containing micro-catalysts.

Some representative pressure traces can be seen in Figs. 31-34, which show representative examples of the pressure traces collected in the lower, middle, and upper pressure regions. The two pressure traces in Figs. 31 and 32 illustrate representative anomalous burning behavior. Pressure traces collected in these lower-pressure regions did not display a linear pressure increase with time, but plateaued in the middle of the combustion process and then continued to increase linearly until the combustion process terminated. The two pressure traces in Figs. 33 and 34 illustrate normal burning behavior. Anomalous burning behavior was confirmed with high-speed video analysis, where the pellet is generally noted to undergo sporadic combustion prior to quenching.

The LPDL of AP is generally associated with radiative heat losses at lower pressures [30]. The metal oxides are not effective burning rate catalysts at lower pressures and also serve to remove heat from the reaction, since they are not reacting.

Furthermore, the amount of heat removed from the reaction increases with catalyst concentration. The combination of these observations explains the observed general trend where the LPDL increases to higher pressures as the catalyst concentration is increased.

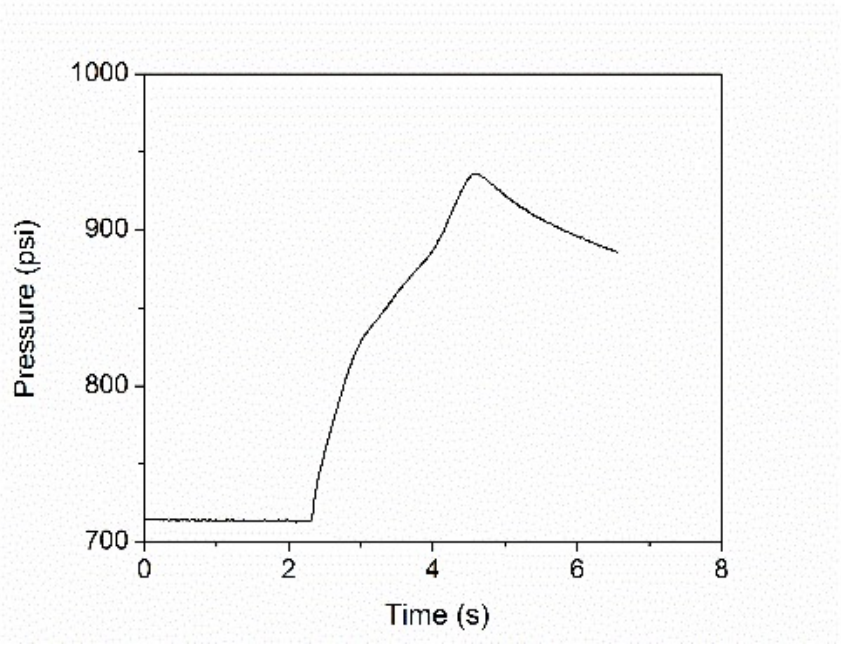

Figure 31 Anomalous pressure trace for a 2% μFe_2O_3 formulation at a test pressure of ~800 psi.

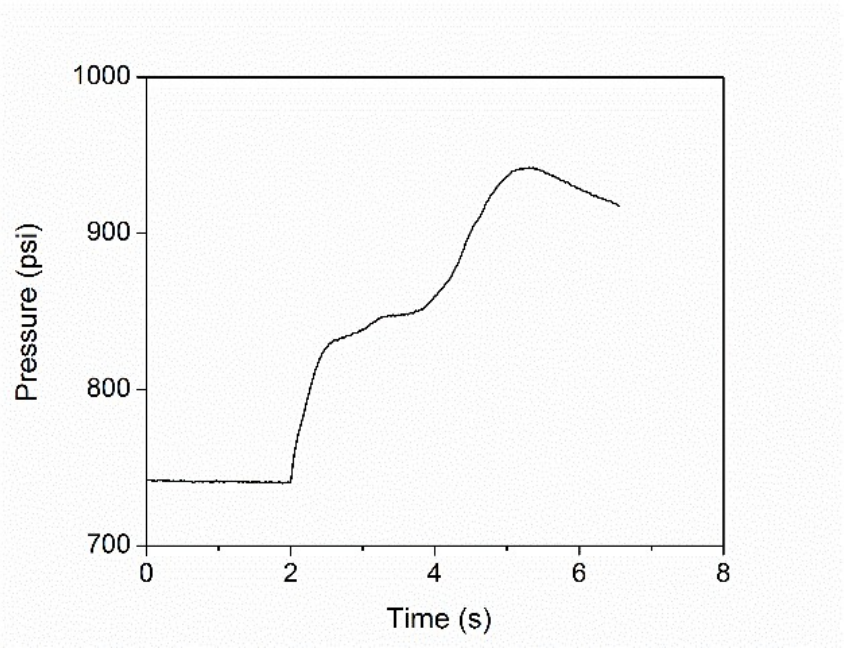

Figure 32 Anomalous pressure trace for a 3% μFe_2O_3 formulation at a test pressure of ~850 psi

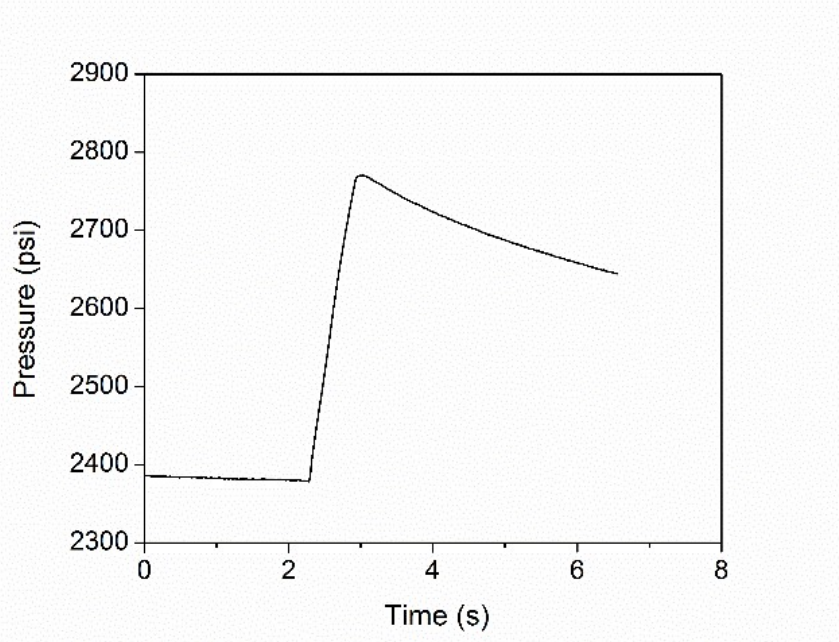

Figure 33 Normal pressure trace for a 1% μFe_2O_3 formulations at a test pressure of ~2,600 psi.

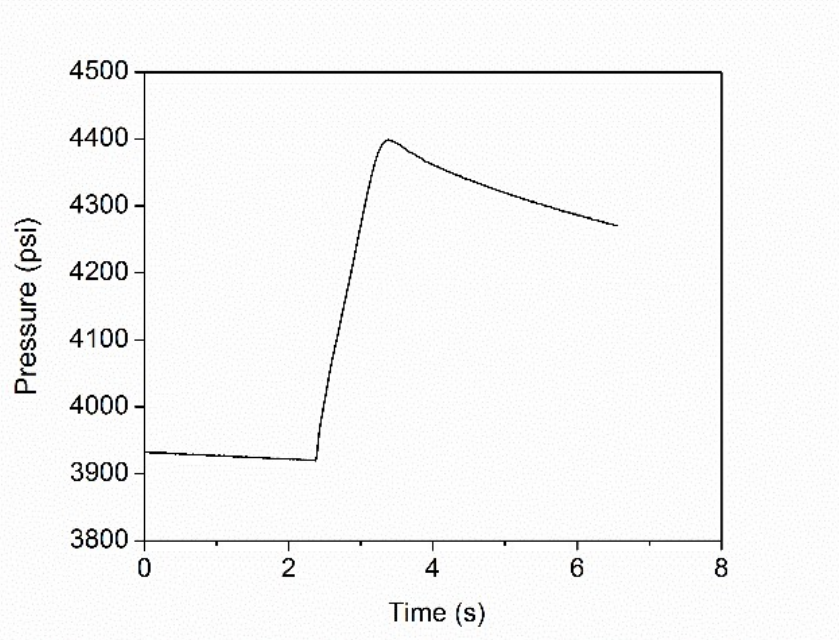

Figure 34 Normal pressure trace for a 2% μTiO_2 formulation at a test pressure of ~4,200 psi.

4.4 Uncertainty Analysis

Uncertainty plays a role in all experiments and can be introduced in different ways such as instrument inaccuracy and human error. The equipment used to take measurements during pellet preparation and data collecting can introduce error in the final calculated value. The length and mass of each pellet were measured using digital calipers and a scientific scale; these pieces of equipment have accuracies of ±0.0005 inches and ±0.01 g, respectively. During the ballistic testing, pressure transducers are used to track the pressure rise in the constant-volume vessel, and the accuracy of these transducers, as reported by the manufacturer, is 0.15%. This inaccuracy correlates to ±0.75 psi at 500 psi experiments and ±7.5 psi when the test pressure reaches 5,000 psi.

The uncertainty of calculating the burning rate is a combination of the measurement error in length using calipers and the human error associated with determining the start and end time of the burn. The start time has a smaller uncertainty than the end time due to the $BKNO_3$ igniting very rapidly and causing a spike in pressure, where at this point the entire top surface of the pellet has been ignited. The end time is going to have a higher uncertainty. A summary of the parameters affecting the burn rate uncertainty and their measurement error can be found in Table 4.

Table 4 Burning rate equation parameters and associated measurement errors.

Parameter	Absolute Measurement Error	Units
Pellet Length (l)	0.002	in
	0.051	mm
Ignition Time (t_1)	0.010	s
Burnout Time (t_2)	0.025	s

The root-sum-square (RSS) method can be used to determine the uncertainty of the burning rate calculation, and Eqn. 2 details the RSS equation generalized to the burning rate equation. Once the derivatives of Eqn. 1 with respect to each variable are taken, the equation will become Eqn. 3.

$$\mu_r = \left[\left(\frac{\partial r}{\partial L}\mu_L\right)^2 + \left(\frac{\partial r}{\partial t_1}\mu_{t_1}\right)^2 + \left(\frac{\partial r}{\partial t_2}\mu_{t_2}\right)^2\right]^{\frac{1}{2}} \quad \textbf{(2)}$$

$$\mu_r = r\left[\left(\frac{\mu_L}{L}\right)^2 + \left(\frac{\mu_{t_1}}{t_2 - t_1}\right)^2 + \left(\frac{\mu_{t_2}}{t_2 - t_1}\right)^2\right]^{\frac{1}{2}} \quad \textbf{(3)}$$

The different values of uncertainty are associated with the start and end time section. Combustion fluctuations and nonlinear pressure trances are the two main ways that the human error can increase. A summary of the burning rate measurement error statistics is shown in Table 5.

Table 5 Burning rate uncertainty error analysis statistics.

Burning Rate Measurement Error Statistics			
Units	(in/s)	(mm/s)	(%)
Average	0.019	0.48	2.93
Standard Deviation	0.016	0.40	1.29
Maximum	0.080	2.03	6.60
Minimum	0.001	0.03	0.82

The minimum and maximum burning rate error for these experiments was found to be 0.82% and 6.60%, respectively. The average error in burning rate for all ballistic testing is 2.93%. Representative error bars can be seen in Fig. 22.

As previously mentioned, a TMD above the threshold of 98% was desirable for AP pellet samples. Low theoretical densities can be attributed to voids and cracks in the samples which may artificially increase burning rate. Sample densities are detailed in Table 1 and are within 2.3% TMD for all formulations. This value is slightly lower than the desired 98% for some formulations, but it is an acceptable range.

5. CONCLUSION AND RECOMMENDATIONS*

Catalytic additives were successfully incorporated into plain AP and manufactured into pellets. All pellets (0.5" × 0.5") were tested over a pressure range of 3.45 to 34.5 MPa (500-5,000 psi). μFe_2O_3 was incorporated at 0.5-3% mass concentrations, while μTiO_2 was incorporated at 1-3% mass concentrations. Thorough characterization of all additives and pellets containing these additives was completed using SEM, TEM, and EDS methods. The 1% mass loading of both catalysts showed the highest burning rate with respect to like-additive formulations. The 1% μFe_2O_3 formulation showed the highest global burning rate enhancement across all formulations.

Catalytic nano-additives (nFe_2O_3 and $nTiO_2$) were successfully incorporated into plain AP and manufactured into pellets with mass loadings of 0.25-1%. The change in mass concentration within the evaluated range did not yield a measurable change in burning rate for either additive. The nFe_2O_3 formulation exhibited higher burning rates relative to the $nTiO_2$ formulations. All additives were ineffective catalysts at lower pressures, but did increase the burning rate at higher pressures.

The current study was successful in producing a previously unavailable dataset of catalyst-loaded AP burning rates with well-characterized additives and has improved the community's understanding of catalyst effects on AP decomposition and combustion

* Parts of this section is reprinted from "Burning Rate Characterization of Ammonium Perchlorate Pellets Containing Catalytic Additives" with permission from Rodriguez, F. A., AIAA 2019-4440, 2019 AIAA Joint Propulsion Conference, Indianapolis, IN, 2019, and from "Burning Rate Characterization of Ammonium Perchlorate Pellets Containing Nano-Catalytic Additives" with permission from Rodriguez, F. A., AIAA 2020-1425, 2020 AIAA Science and Technology Conference, Orlando, FL, 2020.

behavior. However, there are still numerous aspects of AP combustion and catalyst action thereon that need to be explored to obtain a full understanding of AP and AP-based propellant combustion behavior. Accordingly, the author has several recommendations for the community which are discussed, as follows:

The comparisons made between the data available in the literature and the current study demonstrated qualitative, but not quantitative agreement. This finding may be related to the characteristics (composition, crystal structure, size, morphology, etc.) of the additives utilized in the current and previous studies. For example, several references [15,19] demonstrated that a change in additive morphology or manufacturer significantly altered the burning rate of additive-loaded AP. Accordingly, the author recommends that all future studies make an effort to fully characterize both the additives incorporated in samples and the samples with additives included. Full characterization of the additives implemented in such studies would allow for a more complete understanding of what factors influence the reported results.

The combustion behavior of plain AP is still not well-characterized at elevated pressures (>1,800 psi) and development of a first-principles model potentially including fundamental thermodynamics, heat transfer, and/or chemical kinetics could yield a better understanding of the fundamental mechanisms causing the observed results and would be beneficial to the community.

Lastly, the trends observed herein for AP pellets containing catalytic additives generally agree with trends observed in the literature for AP-based propellants loaded with similar additives. However, the author proposes that an experimental study

conducted at a single laboratory facility spanning the combustion analysis of additive-loaded AP pellets, propellant strands, and laminate propellant samples (i.e. ‘sandwich’ propellants) could further elucidate the underlying phenomena surrounding the action of catalytic additives on propellant decomposition and combustion.

REFERENCES

[1] Sutton,G. P., Biblarz, O., Rocket Propulsion Elements. 9th ed. New Jersey: John Wiley & Sons, Inc.; 2017.

[2] Thomas, J. C., Sammet, T. E., Dillier, C. A. M., Demko, A. R., Rodriguez, F. A., Petersen, E. L., "Aging Effects on the Burning Rates of Composite Solid Propellants with Nano-Additives," Journal of Propulsion and Power, Vol. 35, No. 2, 2019, pp. 342-351.

[3] Demko, A.R., Dillier, C., Sammet, T., Petersen, E. L., Reid, D. L., Seal, S., "Ignition Delay Times of Composite Solid Propellants Using Novel Nano-Additive Catalysts," Journal of Propulsion and Power, Vol. 34, No. 5, 2018, pp. 1285-1296.

[4] Demko, A. R., Allen, T. W., Dillier, C., Sammet, T., Petersen, E. L., Reid, D. L., Seal, S., "Temperature Sensitivity of Composite Propellants Containing Novel Nano-Additive Catalysts," Journal of Propulsion and Power, Vol. 34, No. 3, 2018, pp. 795-807.

[5] Demko, A. R., Allen, T. W., Thomas, J. C., Johnson, M., Morrow, G. R., Reid, D. L., Seal, S., Petersen, E. L., "Comparison of Commercially Available and Synthesized Titania Nano-Additives in Composite HTPB/AP Propellant," Propellants, Explosives, Pyrotechnics, Vol. 42, Issue 2, 2017, pp. 158-166.

[6] Thomas, J. C., Demko, A.R., Sammet, T. E., Reid, D. L., Seal, S., Petersen, E. L., "Mechanical Properties of Composite AP/HTPB Propellants Containing Novel Titania Nanoparticles," Propellants, Explosives, Pyrotechnics, Vol. 41, 2016, pp. 822-834.

[7] Grossman, K. D., Sakthivel, T. S., Dillier, C., Petersen, E. L., Seal, S., "Effect of Amine-Modified Boron Nitride (BN) on Ammonium Perchlorate Decomposition," RSC Advances, Vol. 6, 2016, pp. 89635-89641.

[8] Draper, R. E., Reid, D. L., Sakthivel, T. S., Sammet, T., Demko, A., Petersen, E. L., Seal, S., "Facile Nanoparticle Dispersion Detection in Energetic Composites by Rare Earth Doped in Metal Oxide Nanostructures," RSC Advances, Vol. 5, 2015, pp. 68305-68313.

[9] Reid, D., Draper, R., Richardson, D., Demko, A., Allen, T., Petersen, E., Seal, S., "In-Situ Synthesis of Polyurethane—TiO2 Nanocomposite and Performance in Solid Propellants," Journal of Materials Chemistry A, Vol. 2, 2014, pp. 2313-2322.

[10] Krietz, K., Petersen, E., Reid, D., Seal, S., "Scale-up Effects of Nanoparticle Production on the Burning Rate of Composite Propellant," Combustion Science and Technology, Vol. 184, 2012, pp. 750-766.

[11] Reid, D. L., Krietz, K. R., Stephens M. A., King, J. E. S., Nachimuthu, P., Petersen, E. L., Seal, S., "Development of Highly Active Titania-Based Nanoparticles for Energetic Materials," Journal of Physical Chemistry C, Vol. 115, No. 21, 2011, pp. 10412-10418.

[12] Stephens, M., Sammet, T., Petersen, E., Carro, R., Wolf, S., Smith, C., "Performance of Ammonium-Perchlorate-Based Composite Propellant Using Nanoscale Aluminum," Journal of Propulsion and Power, Vol. 26, No. 3, 2010, pp. 461-466.

[13] Stephens, M. A., Petersen E. L., Carro, R., Reid, D. L., Seal, S., "Multi-Parameter Study of Nanoscale TiO2 and CeO2 Additives in Composite AP/HTPB Solid Propellants," Propellants, Explosives, Pyrotechnics, Vol. 35, Issue 2, 2010, pp. 143-152.

[14] Stephens, M. A., Petersen E. L., Reid, D. L., Carro, R., Seal, S., "Nano Additives and Plateau Burning Rates in Ammonium-Perchlorate-Based Composite Solid Propellants," Journal of Propulsion and Power, Vol. 25, No. 5, 2009, pp. 1068-1078.

[15] Reid, D. L., Russo, A. E., Carro, R. V., Stephens, M. A., LePage, A. R., Spalding, T. C., Petersen, E. L., Seal, S., "Nanoscale Additives Tailor Energetic Materials," Nano Letters, Vol. 7, No. 7, 2007, pp. 2157-2161.

[16] Yan, Q., Zhao, F., Kuo, X., Zeman, S., DeLuca, L., "Catalytic effects of nano additives on decomposition and combustion of RDX-, HMX-, and AP-based energetic compositions," Progress in Energy and Combustion Science, 2016, pp. 75-136.

[17] Wang, Y., Xia, X., Zhu, J., Li, Y., Wang, X., and Hu, X., "Catalytic Activity of Nanometer-Sized CuO/Fe2O3 on Thermal Decomposition of AP and Combustion of AP-Based Propellants," Combustion Science and Technology, 2010, pp. 154-162.

[18] Kshisagar, D. R. Jain, S., Bhandarkar, S., Vemuri, M., Mehilal., "Studies on the Effects of Nano-MnO2 in HTPB-based Composite Propellant Formulations," Central European Journal of Energetic Material, Vol. 14, 2017, pp. 589-604.

[19] Marothiya, G., Vijay, C., Ishitha, K., Ramakrishna, P. A., “An effective method to embed catalysts on AP and its effects on the burning rate of aluminized composite solid propellants,” Combustion and Flame, Vol. 182, 2017, pp. 114-121.

[20] Stephens, M., Sammet, T. E., Petersen, E. L., Carro, R., Wolf, S., Smith, C., “Performance of Ammonium-Perchlorate Based Composite Propellants Containing Nanoscale Aluminum,” Journal of Propulsion and Power, Vol. 26, 2010, pp. 461-466.

[21] Friedman, R., et al., “Deflagration of Ammonium Perchlorate,” Proceedings of the Combustion Institute, Vol. 6, 1957, pp. 612-618.

[22] Boggs, T. L., et al., “Combustion of Ammonium Perchlorate and Various Inorganic Additives”, J. Propulsion, Vo. 4, 1988

[23] Mathothiya, G., Vijay, C., Ishitha, K., Ramakrishna, P. A.,” An effective method to embed catalyst on AP and its effect on the burn rates of aluminized composite solid propellants,” Combustion and Flame, Vo. 182, 2017, pp. 114-121.

[24] Seetharamacharyulu, D., Pai Verneker, V. R., and Mallya, R. M., “Defect Sensitization of Combustion and Thermal Decomposition of Ammonium Perchlorate: Effect of Pelletizing Pressure and Dwell Time,” Combustion Science and Technology, Vol. 28, 1982, pp. 41-53.

[25] Tykol, A. J., Burning Rate Characterization of Guanidine Nitrate and Basic Copper Nitrate Propellants with Nano- and Micron-sized Metal Oxide Additives', M.S., Texas A&M University, 2018.

[26] Sinha, A. K., Defects and Distortion in Heat-Treated Parts. Vol. 4. ASM Handbook

Committee; 1991.

[27] Carro RV. High Pressure Testing of Composite Solid Rocket Propellant: Burner Facility Characterization. MS Thesis, Dept. of Mechanical Material and Aerospace Engineering, University of Central Florida, Orlando, Florida, 2007.

[28] Carro R, Stephens M, Arvanetes J, Powell A, Petersen E, Smith C. High-Pressure Testing of Composite Solid Propellant Mixtures: Burner Facility Characterization. 41st AIAA/ASME/SAE/ASEE Jt Propuls Conf Exhib 2005:1–9.

[29] Petersen, E. D., Rodriguez, F. A., Dillier, C. A. M., Thomas, J. C., and Petersen, E. L., “Combustion Behavior of Ammonium Perchlorate at High Pressures,” AIAA 2019-4366, 2019 AIAA Joint Propulsion Conference, Indianapolis, IN, 2019.

[30] Levy, J. B. and Friedman, R., "Further Studies of Pure Ammonium Perchlorate Deflagration," Proceedings of the Combustion Institute, Vol. 8, 1961, pp. 663-672.

APPENDIX A

A-1: Machine drawing of custom sample holder